SPECIAL
Advances in Drought Monitoring
COLLECTION

Assimilation of Remotely Sensed Soil Moisture and Snow Depth Retrievals for Drought Estimation

SUJAY V. KUMAR,* CHRISTA D. PETERS-LIDARD,+ DAVID MOCKO,# ROLF REICHLE,@ YUQIONG LIU,& KRISTI R. ARSENAULT,* YOULONG XIA,** MICHAEL EK,++ GEORGE RIGGS,## BEN LIVNEH,@@ AND MICHAEL COSH&&

* *Science Applications International Corporation, McLean, Virginia, and Hydrological Sciences Laboratory, NASA Goddard Space Flight Center, Greenbelt, Maryland*
\+ *Hydrological Sciences Laboratory, NASA Goddard Space Flight Center, Greenbelt, Maryland*
\# *Science Applications International Corporation, McLean, Virginia, and Global Modeling and Assimilation Office, and Hydrological Sciences Laboratory, NASA Goddard Space Flight Center, Greenbelt, Maryland*
@ *Global Modeling and Assimilation Office, NASA Goddard Space Flight Center, Greenbelt, Maryland*
& *Earth System Science Interdisciplinary Center, University of Maryland, College Park, College Park, and Hydrological Sciences Laboratory, NASA Goddard Space Flight Center, Greenbelt, Maryland*
** *I. M. Systems Group, Inc., and NOAA/NCEP/Environmental Modeling Center, College Park, Maryland*
++ *NOAA/NCEP/Environmental Modeling Center, College Park, Maryland*
Science Systems and Applications, Inc., Lanham, and Cryospheric Sciences Branch, NASA Goddard Space Flight Center, Greenbelt, Maryland
@@ *Cooperative Institute for Research in Environmental Sciences, Boulder, Colorado*
&& *Hydrology and Remote Sensing Laboratory, Agricultural Research Service, USDA, McLean, Virginia*

(Manuscript received 1 August 2013, in final form 13 May 2014)

ABSTRACT

The accurate knowledge of soil moisture and snow conditions is important for the skillful characterization of agricultural and hydrologic droughts, which are defined as deficits of soil moisture and streamflow, respectively. This article examines the influence of remotely sensed soil moisture and snow depth retrievals toward improving estimates of drought through data assimilation. Soil moisture and snow depth retrievals from a variety of sensors (primarily passive microwave based) are assimilated separately into the Noah land surface model for the period of 1979–2011 over the continental United States, in the North American Land Data Assimilation System (NLDAS) configuration. Overall, the assimilation of soil moisture and snow datasets was found to provide marginal improvements over the open-loop configuration. Though the improvements in soil moisture fields through soil moisture data assimilation were barely at the statistically significant levels, these small improvements were found to translate into subsequent small improvements in simulated streamflow. The assimilation of snow depth datasets were found to generally improve the snow fields, but these improvements did not always translate to corresponding improvements in streamflow, including some notable degradations observed in the western United States. A quantitative examination of the percentage drought area from root-zone soil moisture and streamflow percentiles was conducted against the U.S. Drought Monitor data. The results suggest that soil moisture assimilation provides improvements at short time scales, both in the magnitude and representation of the spatial patterns of drought estimates, whereas the impact of snow data assimilation was marginal and often disadvantageous.

1. Introduction

Drought is one of the costliest environmental disasters and has profound socioeconomic consequences, as it typically occurs at long time scales and in virtually all climatic zones. Droughts are generally classified into three physical types: meteorological drought resulting from precipitation deficits, agricultural drought due to total soil moisture deficits, and hydrological drought related to the shortage of streamflow or runoff (Keyantash and Dracup 2002; Mo 2008; Shukla and Wood 2008). The accurate determination of soil moisture states is important not only

Corresponding author address: Sujay Kumar, Hydrological Sciences Laboratory, NASA GSFC, Code 617, Greenbelt, MD 20771.
E-mail: sujay.v.kumar@nasa.gov

DOI: 10.1175/JHM-D-13-0132.1

© 2014 American Meteorological Society

for the characterization of agricultural drought, but also for hydrologic droughts, since the knowledge of initial soil moisture states also influences the predictability of runoff fields (Koster et al. 2014; Mahanama et al. 2008). In addition to soil moisture, snow conditions also play an important role in contributing to the skill of streamflow predictions (Wood et al. 2005; Berg and Mulroy 2006; Koster et al. 2010). In many mid- and high-latitude regions, the seasonal water storage and the associated spring snowmelt dominate the local hydrology. Snowpack in the western United States, for example, is the largest component of water storage (Mote et al. 2005) and is the primary source of water supply. Maurer and Lettenmaier (2003) examined the importance of initial soil moisture and snow states toward the predictability of runoff fields. Their results showed that these states contribute significantly to runoff predictability at seasonal time scales. The accurate determination of moisture storages of soil moisture and snow conditions, therefore, is critical for supporting agriculture and water resources needs in the context of drought mitigation (Pomeroy and Gray 1995; Ffolliott et al. 1989; Barnett et al. 2005; Bales et al. 2006; Franz and Sorooshian 2008).

Unfortunately, long-term spatially and temporally continuous records of snow and soil moisture states are not available in many parts of the world. Both in situ and remote sensing measurements of these variables are available from many observation networks and satellites, and several studies have shown their utility for improving runoff estimation (Rango et al. 1977; Ferguson 1985; Yang et al. 2007). These datasets, however, are typically discontinuous in their spatial and temporal coverages and are subject to uncertainties because of errors in the retrieval models and instrument noise. An alternate approach for runoff estimation is the use of land surface models (LSMs) forced with observed meteorology, which generate spatially and temporally continuous estimates of land surface conditions (Mitchell et al. 2004; Rodell et al. 2004; Kumar et al. 2006). The gridded runoff can be subsequently routed to generate estimates of streamflow, and several studies provide descriptions and evaluations of these approaches (Schlosser et al. 1997; Nijssen et al. 1997; Boone et al. 2004; Lohmann et al. 2004; Zaitchik et al. 2010; Xia et al. 2012c). These studies note that the model-based estimates suffer from uncertainties in the forcing inputs, model parameters, and model structural errors. Data assimilation (DA) techniques have been employed as an effective strategy to combine the strengths of both modeling and observations to generate superior estimates by appropriately weighting their respective sources of errors (Reichle 2008).

There have been several studies that have examined the assimilation of soil moisture and snow observations into land surface models and that have demonstrated that model-simulated soil moisture can be improved through the assimilation of passive microwave soil moisture retrievals (e.g., Margulis et al. 2002; Reichle et al. 2007; Q. Liu et al. 2011; Draper et al. 2012; Nagarajan et al. 2012; Hain et al. 2012). These studies demonstrate improvements not only in near-surface soil moisture fields, but also in fields that are connected to the observations through modeled processes, such as root-zone soil moisture. Peters-Lidard et al. (2011) demonstrated that the assimilation of passive microwave soil moisture observations can be used to improve estimates of evapotranspiration. A number of studies have focused on enhancing runoff prediction through the assimilation of remotely sensed soil moisture. The assimilation of data from a passive microwave radiometer was found to improve the correlation between antecedent soil moisture and subsequent storm-scale runoff ratios (Crow et al. 2005). Other studies (Pauwels et al. 2002; Parajka et al. 2006) reported marginal improvements in runoff estimates from the assimilation of scatterometer soil moisture data.

Snow DA includes the assimilation of snow fraction products (e.g., Rodell and Houser 2004; Slater and Clark 2006; Zaitchik and Rodell 2009; Arsenault et al. 2013) and snow water equivalent (SWE) and snow depth products (e.g., Andreadis and Lettenmaier 2006; Liu et al. 2013). Compared to the visible or near-infrared-based snow cover fraction (SCF) products, the passive microwave–based SWE or snow depth products are typically coarser in resolution and lower in accuracy (Foster et al. 2005; Dong et al. 2005). As a result, studies that employ the assimilation of passive microwave–based retrievals have reported only limited success (Andreadis and Lettenmaier 2006; Dong et al. 2007). In a more recent study, De Lannoy et al. (2012) present results from the joint assimilation of both Moderate Resolution Imaging Spectroradiometer (MODIS) SCF retrievals and Advanced Microwave Scanning Radiometer for Earth Observing System (AMSR-E) SWE retrievals over a region near northern Colorado. Marginal improvements through assimilation were observed, with the lack of interannual variations in the AMSR-E SWE retrievals limiting the success of data assimilation.

Several studies have employed the assimilation of remotely sensed snow observations into land surface and hydrological models for improving streamflow predictions (Roy et al. 2010; Thirel et al. 2011; Yatheendradas et al. 2012). Most of these studies employ fractional snow cover extent data for assimilation, and they report improvements in streamflow simulations as a result of assimilation. Dressier et al. (2004) and He et al. (2011) assimilate in situ measurement-based SWE data for assimilation into hydrological models, leading to improved streamflow

simulations. Few studies, however, have reported improved streamflow through the assimilation of passive microwave–based observations within LSMs, partly because of the low skill of these retrievals. Dechant and Moradkhani (2011) examined different scenarios of assimilating brightness temperature observations from AMSR-E and gauge-measured streamflow into the operational SNOW-17 and Sacramento Soil Moisture Accounting models with mixed results. The assimilation of passive microwave–based data alone was unable to significantly improve the streamflow simulations. Similar results are reported in Liu et al. (2013), where improvements in the snow states were reported with the assimilation of bias-corrected snow depth retrievals from AMSR-E, but these improvements did not necessarily translate to improvements in streamflow prediction.

In this article, we present the assimilation of remotely sensed soil moisture and snow depth retrievals into the Noah land surface model covering a time period of 1979–2011 over the continental United States (CONUS) and provide an assessment of their impact toward drought estimation. Retrieval products from a number of microwave instruments are used during this time period, including the Scanning Multichannel Microwave Radiometer (SMMR; 1978–87), the Special Sensor Microwave Imager (SSM/I; since 1987), and AMSR-E (2002–11). To improve the skill and reduce biases in the passive microwave snow depth retrievals, they are augmented with in situ meteorological station–based measurements. The improvements to the soil moisture, snow, and streamflow fields from data assimilation are evaluated by comparing them to a number of independent datasets. Estimates of agricultural and hydrologic drought are generated from the model simulations using root-zone soil moisture– and streamflow-based percentiles, respectively. A quantitative evaluation of the impact of assimilating soil moisture and snow depth data toward the characterization of agricultural and hydrologic droughts is presented by comparing it with available drought percentage area data from the U.S. Drought Monitor (USDM).

The paper is organized as follows. Section 2 provides a brief description of the experiment setup of the assimilation of passive microwave–based retrievals. This section also presents a description of the data sources used in this study. Section 3 contains a description of the DA method used, including details about the bias correction done for both the soil moisture and the snow depth. Section 4 presents the results of the DA experiments, including the evaluation of modeled soil moisture, snow depth, and streamflow fields. Finally, section 5 provides the summary and main conclusions.

2. Approach

In this study, we employ a domain configuration similar to the one used in the North American Land Data Assimilation System (NLDAS) project (Mitchell et al. 2004), which is a multi-institution effort focused on generating high-quality, spatially and temporally consistent LSM datasets from best available observations and model outputs. The NLDAS domain consists of a 1/8° regular latitude–longitude grid centered over the CONUS (25°–53°N, 125°–67°W). The NLDAS project produces an LSM forcing dataset from a daily gauge-based precipitation analysis, bias-corrected shortwave radiation, and surface meteorology reanalysis. This meteorological dataset is then used to drive a number of LSMs to generate hourly model outputs of land surface conditions including fluxes, soil moisture, snow states (snow cover, SWE, and snow depth), runoff, and streamflow. Phase 2 of the NLDAS project (NLDAS-2; Xia et al. 2012b) includes several enhancements over phase 1 to the forcing datasets and generates the model products in near–real time from 1979 to the present. Phase 1 and phase 2 of the NLDAS projects, however, do not employ the assimilation of remotely sensed datasets. In this article, we use the same domain configuration used in the NLDAS project in order to evaluate the added impact of remotely sensed soil moisture and snow depth DA on improving modeled land surface states and subsequent estimates of drought.

All model simulations are conducted using the National Aeronautics and Space Administration (NASA) Land Information System (LIS; Kumar et al. 2006; Peters-Lidard et al. 2007) on the NLDAS gridded domain, using Noah LSM, version 3.3 (Ek et al. 2003). The domain configuration is designed in a manner as similar as possible to the NLDAS-2 Noah model simulations. The simulations are run with a 30-min time step, and the Noah LSM is spun up by running from 1979 to 2012 twice and then reinitializing the model in 1979. Noah LSM is used operationally at the National Centers for Environmental Prediction (NCEP) as the land component of regional and global weather forecasting models and at the Air Force Weather Agency (AFWA) in the offline land analysis system. More recent upgrades to the model have focused on improving the snow physics within Noah (Barlage et al. 2010; Livneh et al. 2010; Wang et al. 2010) by providing modifications to snow albedo, surface roughness, and surface exchange coefficient formulations. These studies demonstrated improvements to the timing and magnitude of seasonal SWE simulations.

To generate routed streamflow estimates from the gridded runoff fields from the LSM, we employ the streamflow routing model used in the Project for

the Intercomparison of Land-surface Parameterization Schemes (PILPS; Lohmann et al. 1998) and in NLDAS-1 (Lohmann et al. 2004) and NLDAS-2 (Xia et al. 2012c) projects. This model routes the modeled runoff from each interior grid cell to the basin outlet using a flow direction mask (Lohmann et al. 2004). The routing model computes the timing of the runoff at the grid outlet and the water transport through the river network. Using a linearized version of the Saint-Venant equation, both within-grid-cell and river-routing contributions are represented with causal functions with nonnegative impulse response characteristics (Lohmann et al. 1996). The water transported out of the grid cell is further routed through the river network to generate estimates of streamflow, using the distributed approach of Lohmann et al. (1998).

Satellite retrievals

Microwave remote sensing measurements have a long legacy of providing estimates of near-surface soil moisture from a number of sensors (Jackson 1993; Njoku and Entekhabi 1996) for several decades. They include the SMMR (1978–87); the SSM/I (since 1987); the Tropical Rainfall Measuring Mission (TRMM) Microwave Imager (TMI; since 1997); the AMSR-E (2002–11); scatterometer-based products from *European Remote Sensing Satellites 1* and *2* (*ERS-1* and *ERS-2*; 1991–2006) and Advanced Scatterometer (ASCAT; since 2007); and more recently, the Soil Moisture Ocean Salinity (SMOS; since late 2009) and Advanced Microwave Scanning Radiometer 2 (AMSR2) on the *Global Change Observations Mission 1–Water* (*GCOM-W1*) satellite and the soon-to-be-launched Soil Moisture Active Passive (SMAP) mission (Entekhabi et al. 2010b). Y. Liu et al. (2011) developed a merged soil moisture product for the period of 1979–2010 by blending data from these different satellite sensors [known as the Essential Climate Variable (ECV) product]. In this study, we employ the ECV product for data assimilation between 1979 and 2002. From 2002 to 2011, we employ the surface soil moisture retrievals from AMSR-E generated using the Land Parameter Retrieval Model (LPRM) developed by the NASA Goddard Space Flight Center (GSFC) and Vrije Universiteit (VU) Amsterdam (Owe et al. 2008).

Similar to soil moisture retrievals, passive microwave radiometry has been used for estimating snow depth and SWE measurements in the last 30 years (Chang et al. 1987; Foster et al. 1997; Pulliainen and Hallikainen 2001; Kelly et al. 2003; Cordisco et al. 2006; Kelly 2009; Tedesco et al. 2010). From 1978 to 1987, snow depth retrievals from the passive microwave data from SMMR on the *Nimbus-7* satellite using the 19- and 37-GHz channels (Chang et al. 1987) are available. A similar product was derived from SSM/I using the Chang et al. (1987) algorithm for the period from 1987 to the present. Passive microwave–based retrievals using several channels (10, 18, 23, 36, and 89 GHz) from AMSR-E (Kelly et al. 2003) on board the NASA *Aqua* satellite are available from 2002 to 2011. The Kelly et al. (2003) algorithm generates snow depth fields first, and SWE is then calculated by multiplying the snow depth fields with a snow density map. The retrieval algorithm employs snow density fields from the datasets of Brown and Braaten (1998) and Krenke (2004). Here we use the following three snow depth products for data assimilation: the SMMR-based retrievals from 1979 to 1987, SSM/I-based retrievals from 1987 to 2002, and AMSR-E–based retrievals from 2002 to 2011. All three products are available at approximately 25-km spatial resolution.

3. Data assimilation method

A one-dimensional ensemble Kalman filter (EnKF; Reichle et al. 2002a) algorithm is used to separately assimilate the soil moisture and snow depth retrievals into the Noah LSM. The EnKF is a widely accepted technique for sequential assimilation of hydrologic variables, and several studies have employed EnKF for the assimilation of soil moisture, skin temperature, and snow observations (Crow and Wood 2003; Reichle et al. 2007; Kumar et al. 2009; Reichle et al. 2010; De Lannoy et al. 2012; Liu et al. 2013). An ensemble size of 12 is used in the simulations with perturbations applied to both meteorological fields and model prognostic fields to simulate uncertainty in the model estimates. We chose 12 as the ensemble size in this experiment on the basis of prior studies (Reichle et al. 2002b, 2007; Kumar et al. 2008, 2009, 2012b) leading up to this work and because the size of the model state vector is small (four Noah soil moisture state variables). The parameters used for these perturbations are listed in Table 1, which are based on earlier DA studies (Kumar et al. 2008, 2009; Peters-Lidard et al. 2011).

Multiple quality-control measures are applied to the soil moisture and snow depth retrievals prior to data assimilation. Similar to the approach of Reichle et al. (2007), Q. Liu et al. (2011), and Peters-Lidard et al. (2011), the soil moisture retrievals from ECV and LPRM that are flagged for being at the edge of the swath; near water bodies; or impacted by dense vegetation, precipitation, frozen ground, snow cover, or radio frequency interference (RFI) are excluded in the assimilation system. Moreover, an additional layer of quality control is applied on the basis of the information from the LSM by excluding the retrievals when the LSM indicated active precipitation, nonzero snow cover, frozen soil, or dense vegetation (when green vegetation fraction is >0.7). The snow depth

TABLE 1. Parameters for perturbations to meteorological forcings and model prognostic variables in the EnKF assimilation experiments.

Variable	Perturbation type	Std dev	Cross correlations with perturbations in			
Meteorological forcings			SW↓	LW↓	PCP	
Downward shortwave (SW↓)	Multiplicative	0.3	1.0	−0.5	−0.8	
Downward longwave (LW↓)	Additive	$50\,\mathrm{W\,m^{-2}}$	−0.5	1.0	0.5	
Precipitation (PCP)	Multiplicative	0.50	−0.8	0.5	1.0	
Noah LSM soil moisture states			sm1	sm2	sm3	sm4
Total soil moisture–layer 1 (sm1)	Additive	$6.0 \times 10^{-3}\,\mathrm{m^3\,m^{-3}}$	1.0	0.6	0.4	0.2
Total soil moisture–layer 2 (sm2)	Additive	$1.1 \times 10^{-4}\,\mathrm{m^3\,m^{-3}}$	0.6	1.0	0.6	0.4
Total soil moisture–layer 3 (sm3)	Additive	$0.60 \times 10^{-5}\,\mathrm{m^3\,m^{-3}}$	0.4	0.6	1.0	0.6
Total soil moisture–layer 4 (sm4)	Additive	$0.40 \times 10^{-5}\,\mathrm{m^3\,m^{-3}}$	0.2	0.4	0.6	1.0
Noah LSM snow states			SWE	snod		
SWE	Multiplicative	0.01	1.0	0.9		
Snow depth (snod)	Multiplicative	0.02	0.9	1.0		

retrievals are excluded when the model skin temperature or top-layer soil temperature is higher than 5°C. In addition, the dense vegetation–related flags are also applied to the snow depth retrievals prior to data assimilation.

Data assimilation methods, including the EnKF, assume that the model and observations are climatologically unbiased and are designed to correct the random errors in the model background. The handling of systematic errors is a key issue in all DA systems, and we employ the following strategies for addressing bias issues in soil moisture and snow depth DA.

a. *Bias correction of soil moisture retrievals*

For soil moisture DA integrations, the biases between the model and the observations are addressed using the commonly followed approach of a priori cumulative distribution function (CDF) scaling (Reichle and Koster 2004; Drusch et al. 2005), where observations are scaled into the model climatology. First, the model CDF and the observation CDF are computed independently using all available data (for ECV using 1980–2010, AMSR-E using 2002–11, and model using 1979–2012) separately for each grid point. The observations are rescaled next, separately for each grid point, such that the CDFs of the rescaled observations and the model match. Thus, the approach corrects all the moments of the distribution regardless of its shape. This approach of rescaling the observations prior to data assimilation has been used in several soil moisture DA studies (Reichle and Koster 2005; Crow et al. 2005; Reichle et al. 2007; Kumar et al. 2009; Q. Liu et al. 2011; Draper et al. 2011). The input observation error standard deviations for the unscaled retrievals are set to be 0.04 and $0.08\,\mathrm{m^3\,m^{-3}}$ for ECV and LPRM, respectively. Similar to the strategy used in Q. Liu et al. (2011), these input observation error standard deviations are scaled by the ratio of the soil moisture time series standard deviation of the Noah LSM to that of the soil moisture retrievals (ECV or LPRM), resulting in observation error standard deviations that are spatially distributed.

b. *Bias correction of snow depth retrievals*

The a priori scaling approach used for soil moisture assimilation essentially assimilates the anomaly information and ignores the mean field skill in the observations. Prior studies (e.g., De Lannoy et al. 2012) found this approach to be less effective for snow DA, possibly because of the low skill of the passive microwave snow retrievals, which are affected by several factors, including errors related to variations in snow physical properties, surface, and the atmosphere (Foster et al. 2005; Markus et al. 2006; Tedesco and Narvekar 2010). The snow retrievals are also prone to large errors in the presence of dense vegetation and water bodies (Foster et al. 2005). Moreover, they have been shown to be less sensitive to thin snow packs (SWE less than around 10 mm) and to saturate for thick snowpacks (SWE above ground 200 mm; Dong et al. 2005). The gauge measurements of snow, on the other hand, are obtained through direct measurements and are often used to calibrate and validate the indirect measurements from remote sensing platforms. In addition, the information from gauge measurements is employed by several operational agencies to augment estimates of snow from airborne satellite platforms and model simulations (Carroll et al. 2001; Bissolli and Maier 2009; Pulliainen 2006; Ross and Brasnett 2010).

Similar to the strategies reported by Brasnett (1999), Drusch et al. (2004), de Rosnay et al. (2013), and Liu et al. (2013), we employ the available in situ snow depth measurements to augment the retrievals from the passive microwave sensors, using the Cressman objective analysis

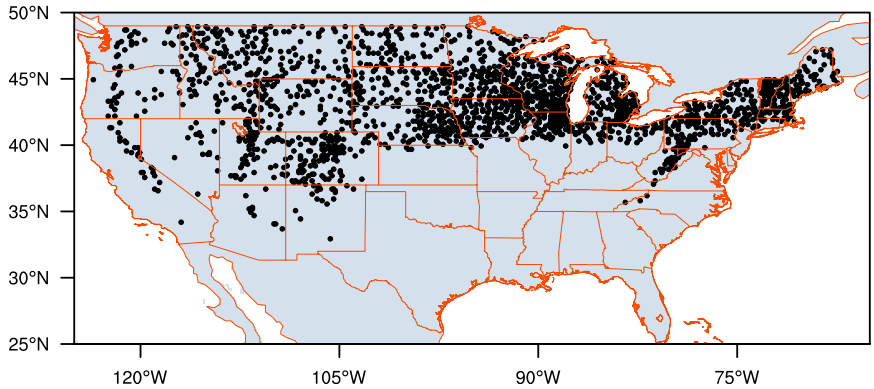

FIG. 1. Location of the GHCN sites used in the Cressman analysis correction of snow depth retrievals.

(Cressman 1959). This technique adjusts the background value (satellite retrievals) by a linear combination of residuals between the station and satellite data. In situ measurements from the Global Historical Climatology Network (GHCN; Menne et al. 2012) meteorological station network are used to generate gauge–satellite merged analyses of snow depth. A number of quality-control procedures are applied to the GHCN data before they are used in the Cressman analysis. The stations are chosen only if they report at least 3 months of valid data during the winter season (December–April) and if they report at least 2 years of data during the 1979–2011 time period. The location of the GHCN stations used in the Cressman analysis is shown in Fig. 1.

The residuals are weighted based on the distance between the grid point of the background data and the grid point of the station data, as shown in Eq. (1):

$$\mathrm{SD}^a = \mathrm{SD}^b + \frac{\sum_{n=1}^{N} w_n(\mathrm{SD}_n^o - \mathrm{SD}_n^{b'})}{\sum_{n=1}^{N} w_n}, \tag{1}$$

where SD_n^o is the in situ snow depth at location n; SD^b is the background snow depth field from the passive microwave sensor; $\mathrm{SD}_n^{b'}$ is the background passive microwave snow depth field at the station location n; and w_n is the weight function, defined as

$$w_n = H(r_n)\upsilon(h_n), \tag{2}$$

where $H(r_n)$ and $\upsilon(h_n)$ are the horizontal and vertical impact functions. Specifically,

$$H(r_n) = \max\left(\frac{r_{\max}^2 - r_n^2}{r_{\max}^2 + r_n^2}, 0\right) \tag{3}$$

and

$$\upsilon(h_n) = \begin{cases} 1 & \text{if} \quad h > 0 \\ \dfrac{h_{\max}^2 - h_n^2}{h_{\max}^2 + h_n^2} & \text{if} \quad -h_{\max} < h_n < 0 \\ 0 & \text{if} \quad h_n < -h_{\max} \end{cases} \tag{4}$$

where $r_{\max}$ is the maximum influence radius defined as 100 km, r_n is the distance between the location of the station n and the background data grid point, $h_{\max}$ is the maximum vertical influence height defined as 300 m, and h_n is the height of the model grid point minus the height (or elevation) of the observing station n. The background data are successively adjusted based on nearby observations through multiple iterations. The maximum radius of influence is reduced on successive iterations in order to build smaller-scale information into the analysis where data density supports it. In the current study, the standard deviation of the observation error is assumed to be 20 mm after bias correction for all three snow depth datasets.

4. Results

This section presents the results from various model and DA integrations. The model simulations are evaluated by comparing them against a number of independent datasets using the Land Surface Verification Toolkit (LVT; Kumar et al. 2012a). Only values at times and locations for which observations are assimilated contribute to the computation of various analysis metrics shown below. Figure 2 shows the effective mask of locations where at least 400 observations are assimilated during the entire simulation period. For streamflow, however, no data masking is employed since the streamflow estimates are influenced by calculations at upstream locations. Furthermore, only grid points with at least 1 yr of assimilated observations during the evaluation period are

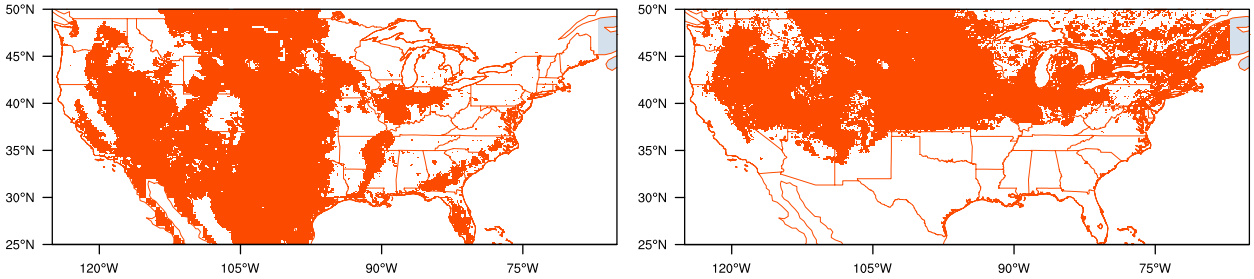

FIG. 2. Effective mask of the locations where at least 1 yr of observations are assimilated: (left) soil moisture DA and (right) snow depth DA.

included in the evaluations, similar to the strategy used in Kumar et al. (2009) and Kumar et al. (2012b). In the soil moisture, snow depth, and streamflow evaluations, we compare the gridbox estimates from the model integrations to point-scale in situ measurements and ignore the impact of spatial scaling errors.

a. Evaluation of soil moisture estimates

The soil moisture estimates from the simulations are compared against two reference datasets: 1) surface soil moisture measurements from four U.S. Department of Agriculture (USDA) Agricultural Research Service (ARS) experimental watersheds (Jackson et al. 2010) and 2) soil profile measurements from the USDA Soil Climate Analysis Network (SCAN; Schaefer et al. 2007). The four ARS watershed networks include Reynolds Creek (Idaho), Walnut Gulch (Arizona), Little Washita (Oklahoma), and Little River (Georgia). The area-averaged surface soil moisture measurements from individual sensor measurements at each watershed are used in this study. The stations in the SCAN network provide hourly soil moisture measurements at soil profile depths of 5, 10, 20, 50, and 100 cm wherever possible. A number of extensive quality-control procedures were applied to the raw data from the SCAN sites, the details of which are described in Q. Liu et al. (2011). We employ this quality-controlled dataset in our evaluations. Figure 3 shows the locations of the four ARS and 60 SCAN stations employed in the evaluations. These sites reflect locations that passed the quality control of the in situ data and where adequate soil moisture observations were assimilated.

Table 2 shows the comparison of the domain-averaged anomaly correlation R, anomaly root-mean-square error (RMSE), and unbiased RMSE (ubRMSE) metrics for the open-loop (OL) and soil moisture DA integrations compared to the ARS and SCAN site data. The associated 95% confidence intervals are computed using the Student's t test (applied temporally to individual sites) and the average confidence interval is reported in Table 2. The anomaly time series for each grid point is estimated by subtracting the monthly-mean climatology values from the daily average raw data, so that the anomalies represent the daily deviations from the mean seasonal cycle. The anomaly R and RMSE values are computed (separately at each grid point), as the correlation coefficient and RMSE between the daily anomalies from the assimilation estimates and the corresponding in situ data, respectively. The ubRMSE metric is computed from the time series after the removal of the long-term mean bias (Entekhabi et al. 2010a). The error metrics are computed for the period from January 2000 to December 2011 when ARS and SCAN measurements are available. In the evaluations, model surface soil moisture is defined as the top 10 cm of the soil column (which is the top soil layer thickness in the Noah LSM), and the measurement at 5 cm is chosen as the observation surface soil moisture. The root-zone soil moisture is defined as the soil moisture content in the top 1 m of the soil column (derived as a suitably weighted vertical average over the model and observation layers).

Table 2 indicates that the open-loop soil moisture estimates show high skill compared to both ARS and SCAN data, likely due to the high-quality, gauge-adjusted precipitation product (Matsui et al. 2010) used to force the LSM integrations. Overall, the improvements obtained from data assimilation are minor and are not statistically significant in some cases. The comparison to the ARS sites indicates that there are improvements in all three metrics because of soil moisture DA, though barely at the statistically significant levels indicated by the 95% confidence intervals that are given for each metric. The average anomaly R for surface soil moisture across the four sites is 0.84, and it increases to 0.86 with soil moisture assimilation. The anomaly RMSE and ubRMSE values for the OL (0.021 and 0.024 $m^3 m^{-3}$, respectively) decrease with assimilation to 0.019 and 0.022 $m^3 m^{-3}$, respectively. The results are still less conclusive in the comparisons to the in situ measurements at the SCAN sites. The domain-averaged anomaly R values do not

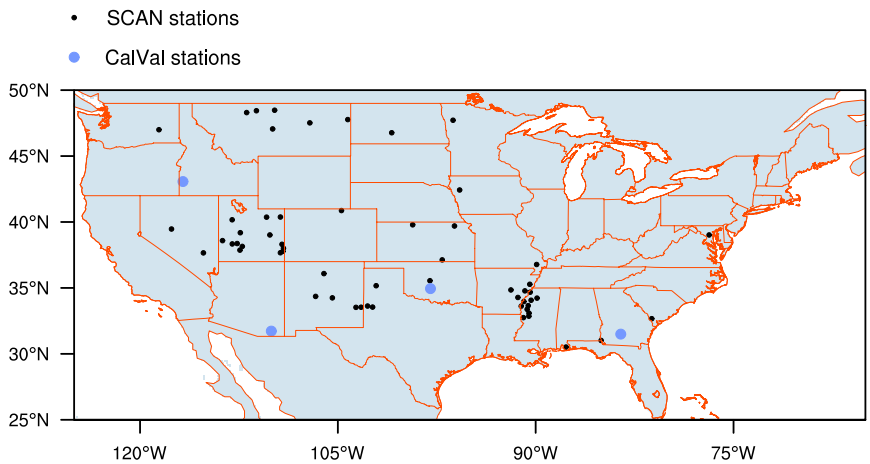

FIG. 3. Location of the ARS and SCAN soil moisture sites used in the soil moisture evaluations.

show a statistically significant improvement or degradation for both surface and root-zone comparisons. The anomaly RMSE and ubRMSE metrics for surface soil moisture estimates decrease with data assimilation, but not at a statistically significant level. Similar trends are seen for the root-zone soil moisture estimates, with marginal improvements in anomaly RMSE and ubRMSE values.

b. *Evaluation of snow depth estimates*

The spatially distributed snow depth estimates from the Canadian Meteorological Centre (CMC) daily snow depth analysis (Brown and Brasnett 2010) and the National Oceanic and Atmospheric Administration (NOAA) National Weather Service's National Operational Hydrologic Remote Sensing Center (NOHRSC) Snow Data Assimilation System (SNODAS; Barrett 2003) outputs are used to evaluate the snow depth fields from model integrations. The CMC analysis is available at approximately 25-km spatial resolution globally from March 1998 to the present. SNODAS data products are generated at 1-km spatial resolution beginning in October 2003 and at hourly temporal resolution over the CONUS. Both the CMC and SNODAS analyses are generated by combining the estimates from a snow model with satellite-derived, airborne, and ground-based observations of snow from surface synoptic observations, meteorological aviation reports, and special aviation reports acquired from the World Meteorological Organization (WMO). A time period from March 1998 to December 2011 is used in the CMC comparisons, and a time period from October 2003 to December 2011 is used in the SNODAS comparisons.

Table 3 presents the domain-averaged RMSE and bias values versus CMC and SNODAS products for the snow depth estimates from the OL and snow depth assimilation integrations, and Fig. 4 shows the seasonal breakdown of these errors. The domain-averaged values are computed from daily RMSE and bias values across all grid points in the domain. The model integration without assimilation has larger errors, and the assimilation helps in improving the snow depth estimates throughout the snow season. More significant improvements are obtained in the peak winter months (December–February) compared to the snow accumulation and melt periods. Table 3 indicates that the error metrics are improved with snow depth DA in both sets of comparisons. The OL integration has a domain-averaged RMSE of 60.8 mm and a domain-averaged bias of 9.8 mm, and they reduce to 54.9 and 0.2 mm, respectively, in the comparisons

TABLE 2. Comparison of domain-averaged anomaly R, anomaly RMSE, and unbiased RMSE of OL and soil moisture DA integrations compared to ARS and SCAN site data (all with 95% confidence intervals). CalVal refers to calibration and validation.

	OL	Soil moisture DA
vs ARS CalVal sites (surface soil moisture)		
Anomaly R	0.84 ± 0.02	0.86 ± 0.02
Anomaly RMSE ($m^3 m^{-3}$)	0.021 ± 0.001	0.019 ± 0.001
ubRMSE ($m^3 m^{-3}$)	0.024 ± 0.002	0.022 ± 0.002
vs SCAN sites (surface soil moisture)		
Anomaly R	0.67 ± 0.02	0.67 ± 0.02
Anomaly RMSE ($m^3 m^{-3}$)	0.037 ± 0.002	0.036 ± 0.002
ubRMSE ($m^3 m^{-3}$)	0.043 ± 0.003	0.041 ± 0.003
vs SCAN sites (root-zone soil moisture)		
Anomaly R	0.60 ± 0.02	0.59 ± 0.02
Anomaly RMSE ($m^3 m^{-3}$)	0.032 ± 0.002	0.030 ± 0.002
ubRMSE ($m^3 m^{-3}$)	0.041 ± 0.003	0.039 ± 0.003

TABLE 3. Comparison of domain-averaged RMSE and bias values of snow depth vs CMC and SNODAS estimates from the OL and DA-SNOW integrations (all with 95% confidence intervals).

	OL	DA-SNOW
vs CMC		
RMSE (mm)	60.8 ± 1.0	54.9 ± 1.0
Bias (mm)	9.8 ± 1.0	0.2 ± 1.0
vs SNODAS		
RMSE (mm)	68.2 ± 1.0	66.3 ± 1.0
Bias (mm)	−22.3 ± 1.0	−19.7 ± 1.0

against CMC. Similarly, in the SNODAS comparisons, both domain-averaged RMSE and bias reduce through data assimilation (the domain-averaged RMSE is reduced from 68.2 to 66.3 mm and the domain-averaged bias is reduced from −22.3 to −19.7 mm). All these differences are statistically significant, as shown by the 95% confidence intervals in Table 3. It was also noticed (not shown) that most major degradations in the simulated snow fields were in the western parts of the domain.

Note that since the GHCN measurements are already used in the bias correction of the snow depth retrievals, we cannot use these same station measurements for evaluating the model integrations. On the other hand, CMC and SNODAS are model-based products that possibly ingest some of the same GHCN stations in their analysis. Nevertheless, we use them to evaluate the model integrations primarily because of the lack of another independent observation data product. These results confirm that the strategy of bias correction through GHCN measurements, and the subsequent improvements obtained through data assimilation are consistent with the both CMC and SNODAS products.

c. *Evaluation of streamflow estimates*

To evaluate the streamflow estimates, we use two reference datasets: 1) daily streamflow data from 1979 to 2012 obtained from the U.S. Geological Survey (USGS; http://nwis.waterdata.usgs.gov/nwis) over 572 small, unregulated basins and 2) monthly "naturalized" streamflow data at 19 major basin outlets (Mahanama et al. 2012), which were developed by removing water management effects. The small basins range in size from 625 km^2, the approximate size of the AMSR-E footprint, up to 10 000 km^2 and had no visible signs of reservoir operation. These basins were also part of the model evaluations used in the NLDAS-2 project (Xia et al. 2012c) and are a subset of the Model Parameter Estimation Experiment (MOPEX) study basins.

1) EVALUATION OVER SMALL CATCHMENTS

Because the magnitude of streamflow estimates varies significantly across different basins, we use a normalized information contribution (NIC) measure to quantify the improvement or degradation due to data assimilation, across different analysis metrics [similar to the approach used in Kumar et al. (2009)]. The NICs for RMSE, R, and Nash–Sutcliffe efficiency (NSE) are defined as follows:

$$\mathrm{NIC}_{\mathrm{RMSE}} = \frac{(\mathrm{RMSE}_o - \mathrm{RMSE}_a)}{\mathrm{RMSE}_o}, \tag{5}$$

$$\mathrm{NIC}_R = \frac{(R_a - R_o)}{(1 - R_o)}, \tag{6}$$

and

$$\mathrm{NIC}_{\mathrm{NSE}} = \frac{(\mathrm{NSE}_a - \mathrm{NSE}_o)}{(1 - \mathrm{NSE}_o)}, \tag{7}$$

where the subscripts o and a denote open loop and assimilation, respectively. Each NIC metric is defined as a measure of how much of the maximum skill improvement [which, in the case of R, is $(1 - R_o)$] is realized through data assimilation [which, in the case of R, is $(R_a - R_o)$]. Note that in the case of RMSE, the NIC metric is defined as the ratio of $(\mathrm{RMSE}_o - \mathrm{RMSE}_a)$ (which is the skill improvement through data assimilation) and RMSE_o, which is the maximum skill improvement. If assimilation improves over the open-loop skill, then the NIC metric will be positive. It will be negative if the assimilation degrades compared to the open loop. For NIC = 0, the assimilation does not add any skill, and for NIC = 1, the assimilation realizes the maximum skill improvement.

Figure 5 presents the NIC values for RMSE, R, and NSE from both soil moisture and snow depth assimilations (relative to the OL integration) and their distribution across the basins. The histograms indicate that improvements in streamflow are minor across most basins and that soil moisture DA on average provides slightly more consistent improvements compared to snow DA (the frequencies of positive NIC values are higher for soil moisture DA, whereas the frequencies of negative NIC values are larger for snow DA). This is also reflected in the domain-averaged NIC values. Though small, the domain-averaged NIC metrics are positive for soil moisture DA for all three metrics. NIC values from snow depth DA, on the other hand, show mixed results. The domain-averaged NIC values for RMSE and NSE from snow DA are negative, indicating overall degradation in these metrics due to snow depth DA. To compute the statistical significance of the NIC values, the 95%

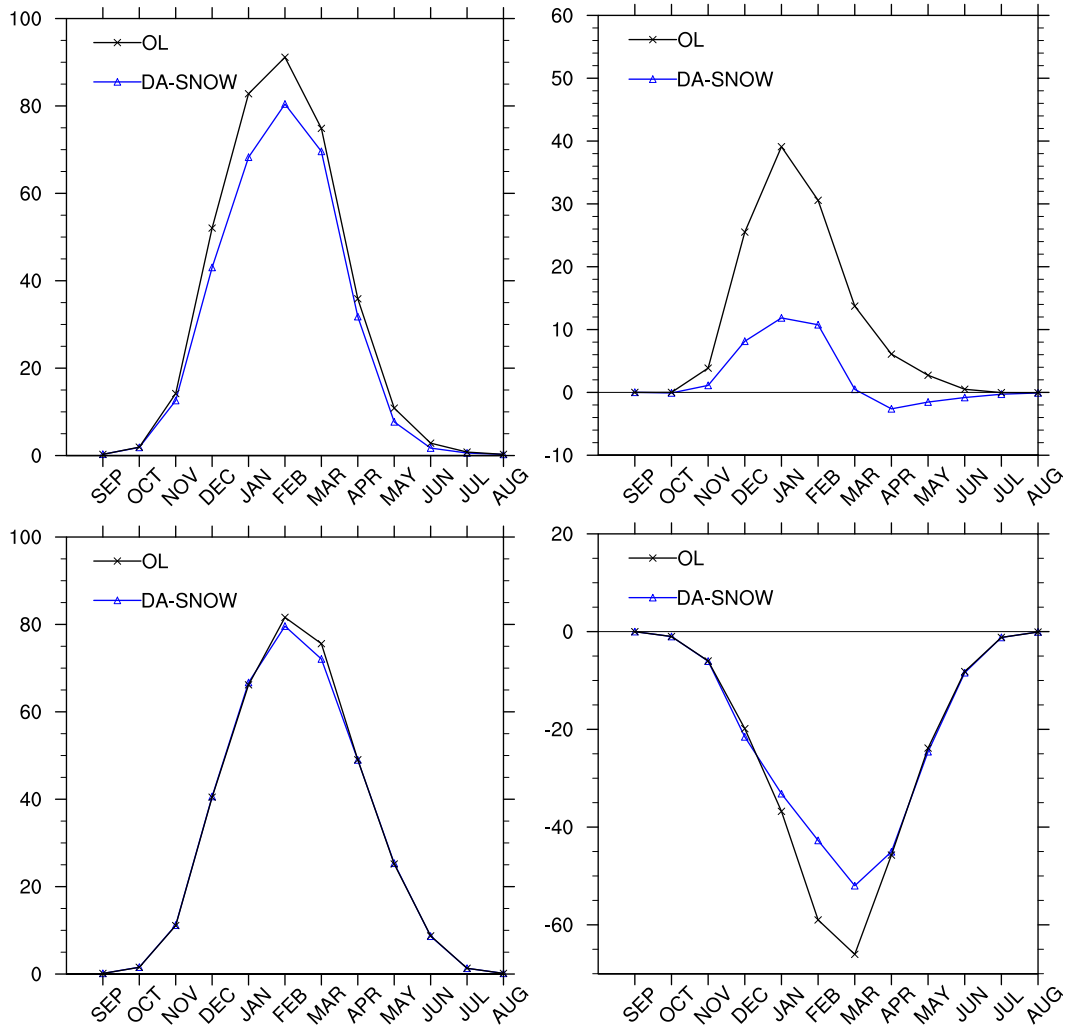

FIG. 4. Average seasonal cycle of (left) RMSE and (right) bias of snow depth estimates (mm) from the OL and snow depth DA (DA-SNOW) integrations compared to the (top) CMC and (bottom) SNODAS products.

confidence intervals of the metrics for the assimilation (δRMSE$_a$, δR_a, and δNSE$_a$) and the OL integrations (δRMSE$_o$, δR_o, and δNSE$_o$) are translated into a corresponding 95% confidence interval for the NIC values (δNIC) using a similar approach as that of Kumar et al. (2009). The 95% confidence intervals computed for the NIC values provide a range of approximately $\pm$0.003–0.08, indicating that the domain-averaged trends shown in Fig. 5 are not always statistically significant.

The variation in the streamflow skill improvements across the domain in Fig. 5 also shows several interesting features, which correlate with the areas of the domain where data assimilation occurs (shown in Fig. 2). As expected, the snow depth retrievals are available over the Midwest, parts of the Northeast, High Plains, and western United States. The soil moisture retrievals are available over parts of the Mississippi basin, Midwest, and western United States. Overall, most improvements from snow depth DA are obtained over parts of the Missouri and upper Mississippi basins and the Northeast. Most notable degradations in streamflow due to snow depth assimilation are observed over the Colorado headwater region and over the northwestern United States. This indicates that the in situ bias correction with GHCN data is still insufficient to provide subsequent skill improvements in streamflow simulations over these areas. In these regions, snow sampling representativeness is a known issue, where the observations considerably undersample the highest elevations, because of logistical constraints. The skill improvements from soil moisture assimilation are mostly over parts of the Mississippi, Missouri and Arkansas–Red basins and parts of the southeastern United States. The NSE values themselves have a large range among these individual basins (not shown). As a result, even the

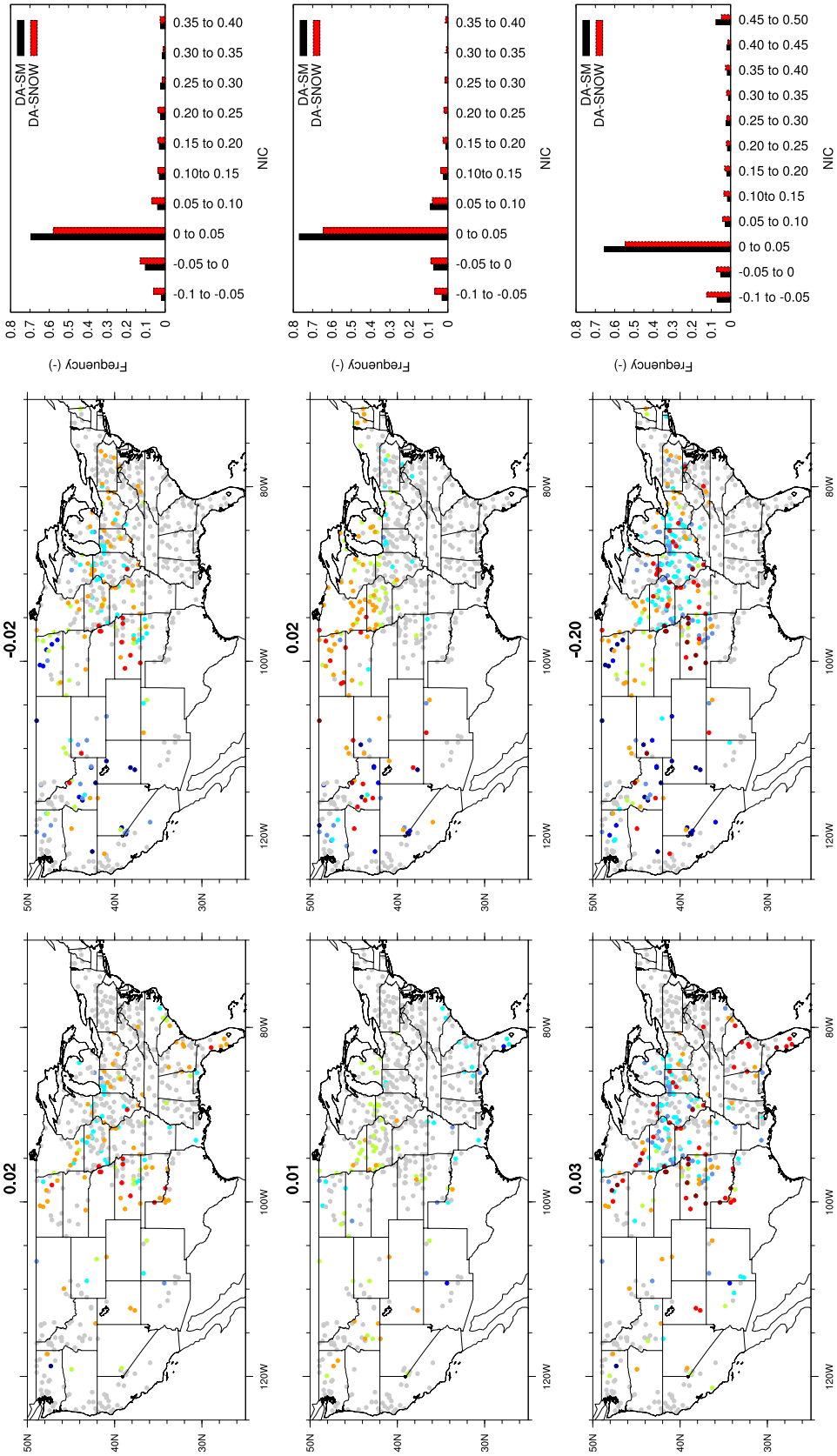

FIG. 5. Streamflow NIC values for (top) RMSE, (middle) correlation coefficient, and (bottom) NSE from (left) soil moisture DA and (middle) snow depth DA. The titles represent the domain-averaged NIC values. Red and blue colors indicate skill improvements and degradations from DA, respectively. (right) The distribution of NIC values for each metric.

TABLE 4. List of the major basins.

Station	River name	Lat (°N)	Lon (°W)	Basin area (km^2)
1 (APA)	Apalachicola River near Sumatra	29.95	85.02	49 728
2 (ALA)	Alabama River near Claiborne	31.55	87.51	56 900
3 (RED)	Red River near Arthur City	33.88	95.50	115 335
4 (PUE)	Rio Puerco near Bernardo	34.41	106.85	19 036
5 (RAL)	Arkansas River near Ralston	36.50	98.73	141 064
6 (LEE)	Colorado River at Lees Ferry	36.87	111.58	289 562
7 (OHI)	Ohio River at Metropolis	37.15	88.74	525 770
8 (UPM)	Upper Mississippi near Grafton	38.90	90.30	443 660
9 (GUN)	Gunnison River near Grand Junction	38.98	108.45	20 533
10 (POT)	Potomac River at Point of Rocks	39.27	77.54	25 000
11 (DEL)	Delaware River near Memorial Bridge	39.69	75.52	28 567
12 (SBB)	Sacramento River near Bend Bridge	40.29	122.19	23 051
13 (GRE)	Green River near Greendale	40.91	109.42	50 116
14 (RAN)	Missouri River at Fort Randall Dam	43.07	98.55	682 465
15 (WIL)	Willamette River near Oregon City	45.34	122.62	25 900
16 (ICE)	Snake River at Ice Harbor Dam	46.25	118.88	281 015
17 (MUS)	Musselshell River near Moseby	46.99	107.89	20 321
18 (GAR)	Garrison Reservoir (Missouri River)	47.39	101.39	469 826
19 (FTP)	Missouri River at Fort Peck Reservoir	48.04	106.36	149 070

normalized NIC metric values show more magnified trends of improvement and degradation, compared to those seen with NIC for RMSE and R.

2) EVALUATION AT MAJOR BASIN OUTLETS

In this section, we present an evaluation of the streamflow estimates at several large basin outlets, where the modeled streamflow estimates are compared against "naturalized" streamflow data (with water management effects removed), similar to the evaluations used in Mahanama et al. (2012). Table 4 lists the details of the major basins examined in this study. Note that the Ohio and Rio Puerco gauges are not naturalized and were selected based on minimal diversion upstream of the gauge.

Figure 6 shows the NIC values for RMSE, R, and NSE at these major basin outlets from soil moisture and snow depth DA. The basins are listed from left to right (in Fig. 6) in the increasing order of their latitude location. The trends in the figure indicate that skill improvements from snow depth DA are generally obtained at higher latitude basin outlets (e.g., Green River, Musselshell, and Missouri River). Soil moisture assimilation also provides skill improvements at several basin outlets, including Apalachicola, Alabama, Willamette, and the Missouri at Garrison, whereas degradations in skill metrics are observed at a few outlets, including Rio Puerco, Red River, Ohio, and the Missouri at Fort Peck. The largest basins (based on basin area) among these are the Missouri at Fort Randall Dam (RAN), Ohio (OHI), Missouri at Garrison (GAR), and upper Mississippi (UPM), which all have basin areas larger than 400 000 km^2. Soil moisture assimilation provides marginal improvements (in R) at Garrison, with marginal degradations at Ohio and upper Mississippi. Except at Garrison, snow DA leads to degradations at all of these large basin outlets.

As noted in Lohmann et al. (2004) and Xia et al. (2012c), the simulated streamflow skills in the NLDAS simulations show large variations across the basins. They reported differences by a factor of up to 4 in modeled runoff relative to the observations at some basins. Similar trends are observed in our results, with large biases observed in the model simulations at some basins such as at Rio Pureco, Ohio, and upper Mississippi (not shown). Figure 7 shows a comparison of the mean seasonal cycles of streamflow at four basin outlets (Missouri at Fort Peck, Gunnison, Green, and Musselshell). Except in the case of the Green River, the impact of data assimilation is very small. At the Green River outlet, snow DA helps in correcting a systematic phase shift possibly due to a late spring snowmelt in the OL simulation. The impact of soil moisture DA, on the other hand, is marginal and is primarily in modifying the bias characteristics of the OL-based streamflow simulation.

d. *Evaluation of drought estimates*

The typical approach to characterizing drought is through normalized indices that capture the deficits of the water cycle variable of interest (e.g., precipitation, soil moisture, or streamflow) from average conditions. As presented in Heim (2002), there is a broad variety of metrics that have been developed for drought quantification, each with its own strengths and weaknesses. In this section, we present an evaluation of the impact of data assimilation on drought estimates through percentile-based drought indices, used in the NLDAS drought monitoring system (Ek et al. 2011; Sheffield et al. 2012). The percentiles are calculated as follows: for the variable

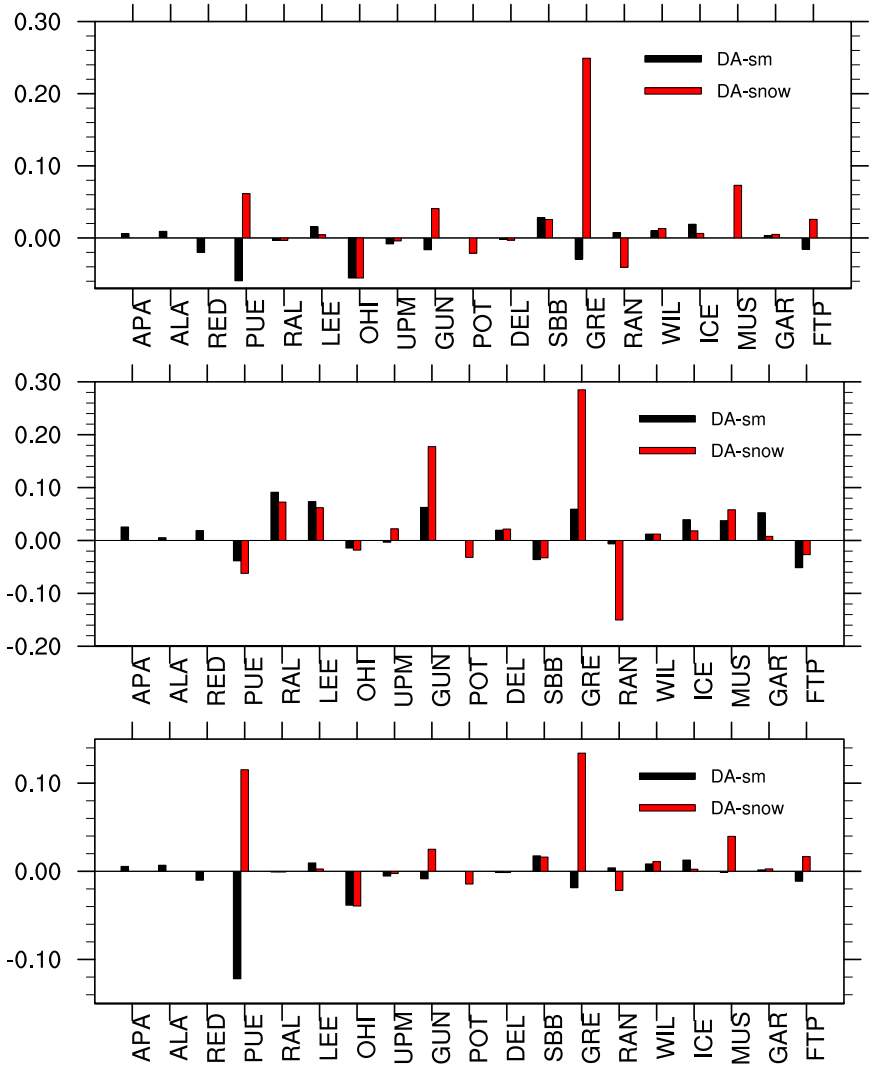

FIG. 6. Streamflow NIC values for (top) RMSE, (middle) correlation coefficient, and (bottom) NSE from soil moisture DA and snow depth DA at major basin outlets listed in Table 4.

of interest (e.g., soil moisture) the climatology is generated first, using daily outputs from 33 yr of model simulations from 1979 to 2011, and for each grid point. The climatology is generated by assembling the variable values for a particular calendar day across all 33 yr. To improve the sampling density and to smooth out the record, a moving window of 5 days is employed. For example, 3 January climatology is assembled by using all the values from 1 to 5 January, across all years (leading to $5 \times 33 = 165$ values for each calendar day). Once the climatology is assembled, the daily percentile values are computed by ranking each day's estimate against the climatology.

Since 1999, the National Drought Mitigation Center (NDMC) has been producing weekly estimates of drought conditions through the USDM (Svoboda et al. 2002). Drought intensity is classified in the USDM into five categories: D0 (abnormally dry, percentile ≤30%), D1 (moderate drought, percentile ≤20%), D2 (severe drought, percentile ≤10%), D3 (extreme drought, percentile ≤5%), and D4 (exceptional drought, percentile ≤2%). In this section, we compare the weekly percentage of area in drought over CONUS from model simulations against data from the USDM archives (http://droughtmonitor.unl.edu/MapsAndData/MapArchive.aspx) for these five categories, during the time period of 2000–11. These weekly drought percentage area values are produced for six different regions of the United States: South, Southeast, Northeast, Midwest, High Plains, and West (as defined in the USDM; Fig. 8).

Root-zone soil moisture estimates are frequently used as leading indicators of agricultural drought (Bolten and

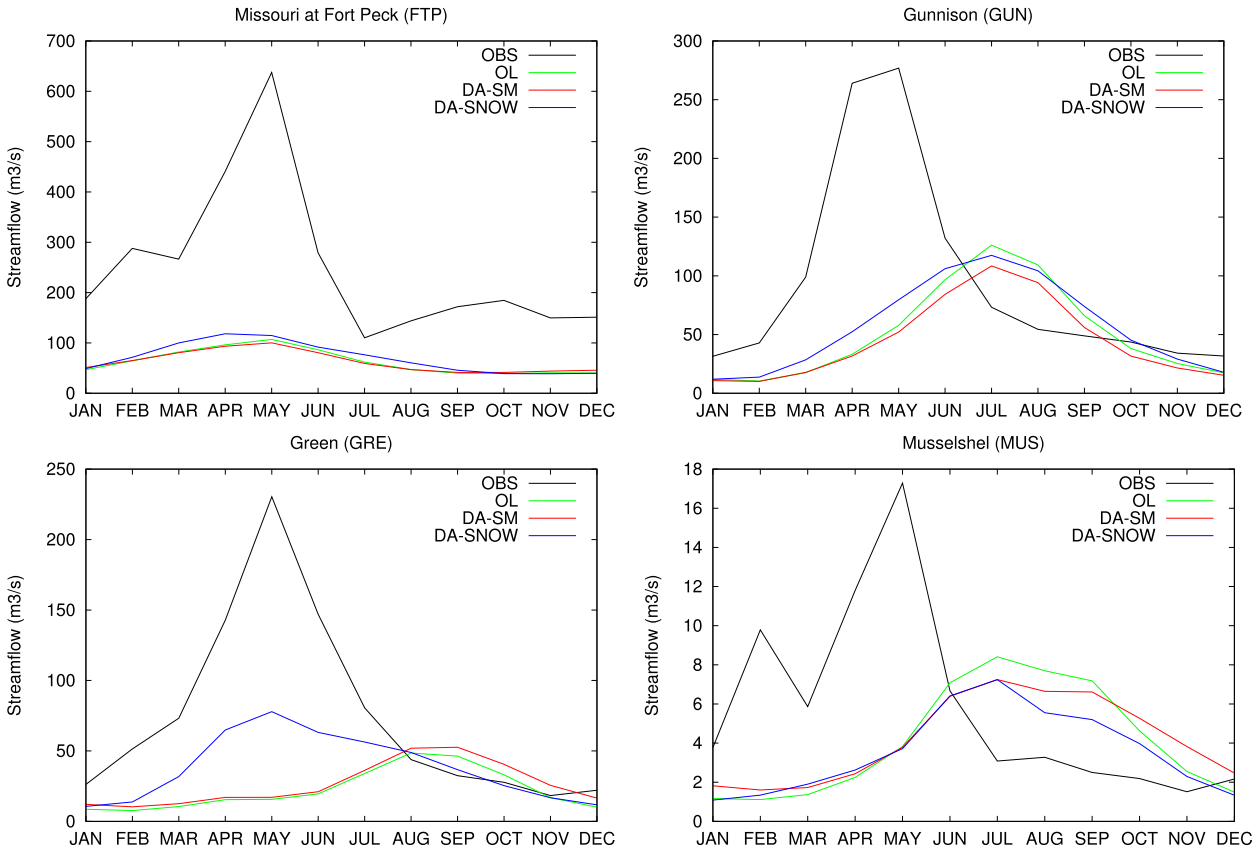

FIG. 7. Mean seasonal cycles of streamflow at the four major basin outlets listed: Missouri at Fort Peck, Gunnison, Green, and Musselshell.

Crow 2012), especially in warm seasons and climates. Figure 9 shows a weekly time series of the drought area percentage based exclusively on root-zone soil moisture percentiles from the OL and DA integrations for the South region of the USDM. We focus on the South region first, since the effect of cold season processes is small, and hence soil moisture percentiles alone are a good proxy for drought, and also because this region provides sufficient soil moisture retrievals for soil moisture DA. The percentage drought area estimates from the OL simulation show high skills, as they match the corresponding drought percentage areas from the USDM throughout the evaluation period and across the five categories. As expected, the snow depth DA does not add any skill to the estimates in this region. Soil moisture DA, on the other hand provides added improvements, most notably in the D0 and D1 drought categories. During the significant drought events in 2006, 2008, and 2011, the drought percentile areas from soil moisture DA are systematically closer to the USDM values, relative to the OL estimates. For more severe drought categories (D2–D4), the added improvements from soil moisture assimilation are marginal.

Quantitative evaluation of the drought area percentage values against the USDM for all six regions is shown in Table 5 using R, RMSE, and bias estimates. The highest skills in R values are observed in the South region (with open-loop R values ranging from 0.73 to 0.91 across different drought categories). The other climate regions also show reasonably high skills, except in a few cases (such as over the Northeast and Midwest for D3 and D4 categories). Though minor, soil moisture DA provides improvements in RMSE and bias for the OL estimates over the South, Southeast, High Plains, and West regions with degradations observed over the Midwest. Even though the metrics in Table 5 generally indicate trends of improvement (for soil moisture DA), only a few are in fact statistically significant (as shown in Table 5 in boldface). The results also indicate that the impact in the root-zone soil moisture–based drought percent area metrics from snow depth DA is small in most regions, with some statistically significant degradation noted over the Midwest and West regions.

Note that soil moisture DA employs the a priori CDF-scaling approach, which rescales the observations into the model's climatology before assimilation. This

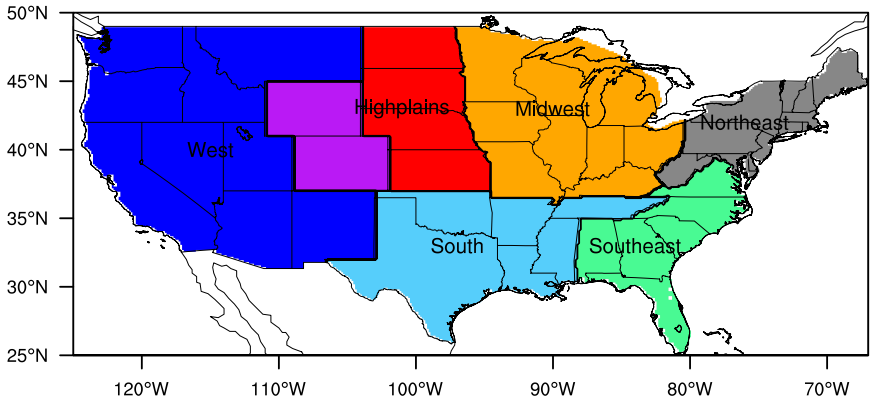

FIG. 8. Six geographical regions of the CONUS defined in the USDM: West, High Plains, Midwest, Northeast, South, and Southeast. Note that the area marked by the purple color is included in both West and High Plains regions (defined by USDM).

ensures that the soil moisture climatology (relative to the OL simulation) does not change in the DA integration and that the influence of data assimilation is only to affect the temporal patterns of the anomalies. As a result, the current assimilation strategy is unlikely to show changes in drought estimates at long time scales relative to the OL predictions and the influence is likely to be more due to the soil moisture variations at shorter time scales (as confirmed by the patterns in Fig. 9).

Similar to Fig. 9, Fig. 10 presents the comparison of weekly hydrological drought estimates computed based on streamflow percentiles (instead of root-zone soil moisture) against the USDM values. The patterns are similar to those observed in Fig. 9, with improvements due to soil moisture DA obtained most prominently in categories D0–D2, indicating that soil moisture DA generally helps in improving the detection of moderate low-flow events. Quantitative statistics similar to Table 5 were also obtained (not shown) for streamflow-percentile-based drought area estimates. No significant improvements in the streamflow-based drought percent area estimates due to snow depth DA were obtained, similar to the results shown in Table 5.

It is important to note that the drought percentage area data from USDM for the D0–D4 designations do not strictly map to a particular type of drought, though in our comparisons we directly compare the root-zone soil moisture– and streamflow-percentile-based drought areas to this data. Soil moisture– and streamflow-based percentiles alone are not necessarily equivalent to USDM (though soil moisture is a good proxy in the South region based on Fig. 9), which uses a blend of indicators in addition to expert judgment. Though the results in Fig. 10 are helpful for illustrating the impacts of data assimilation, we cannot necessarily expect to match the USDM data with the drought area estimates based solely on streamflow.

A comparison of the spatial distribution of drought intensities is presented in Fig. 11 for three cases in the years 2006, 2008, and 2011. The figure shows the drought percentiles from the OL and soil moisture DA integrations against the corresponding drought intensity map obtained from the USDM archives. Maps generated using both root-zone soil moisture– and streamflow-based percentiles are shown in Fig. 11. These figures illustrate the added impact of soil moisture DA for improving drought estimates. For the 18–25 July 2006 case, soil moisture assimilation provides a better estimate of drought severity, especially for D1 and D0 categories (over Texas, Nebraska, and North and South Dakota), consistent with the USDM estimate. For the 2008 case, the DA integration predicts more intense drought over North Dakota and Montana, reduces the severity over Nevada, and increases the spatial extent of drought over Texas and New Mexico, all consistent with the USDM map. Both the model-based estimates do not capture very well the spatial pattern of the intense drought for the 2011 case. Nevertheless, DA-based estimates show increased severity of drought over Texas and Oklahoma relative to the open loop. The streamflow-based drought intensity maps also show similar trends. In all three cases, the OL-based estimates show less severe drought over Texas compared to the USDM, and DA leads to an increase in the drought intensity estimates. In the 2006 case, for example, the OL-based estimate shows most of Texas not even in the D0 category, whereas DA-based estimate indicates increased spatial extent of drought. In these three cases, note that the differences in the drought estimates between the soil moisture DA and OL is higher over Mexico than that over the CONUS (with DA-based estimates generally indicating more

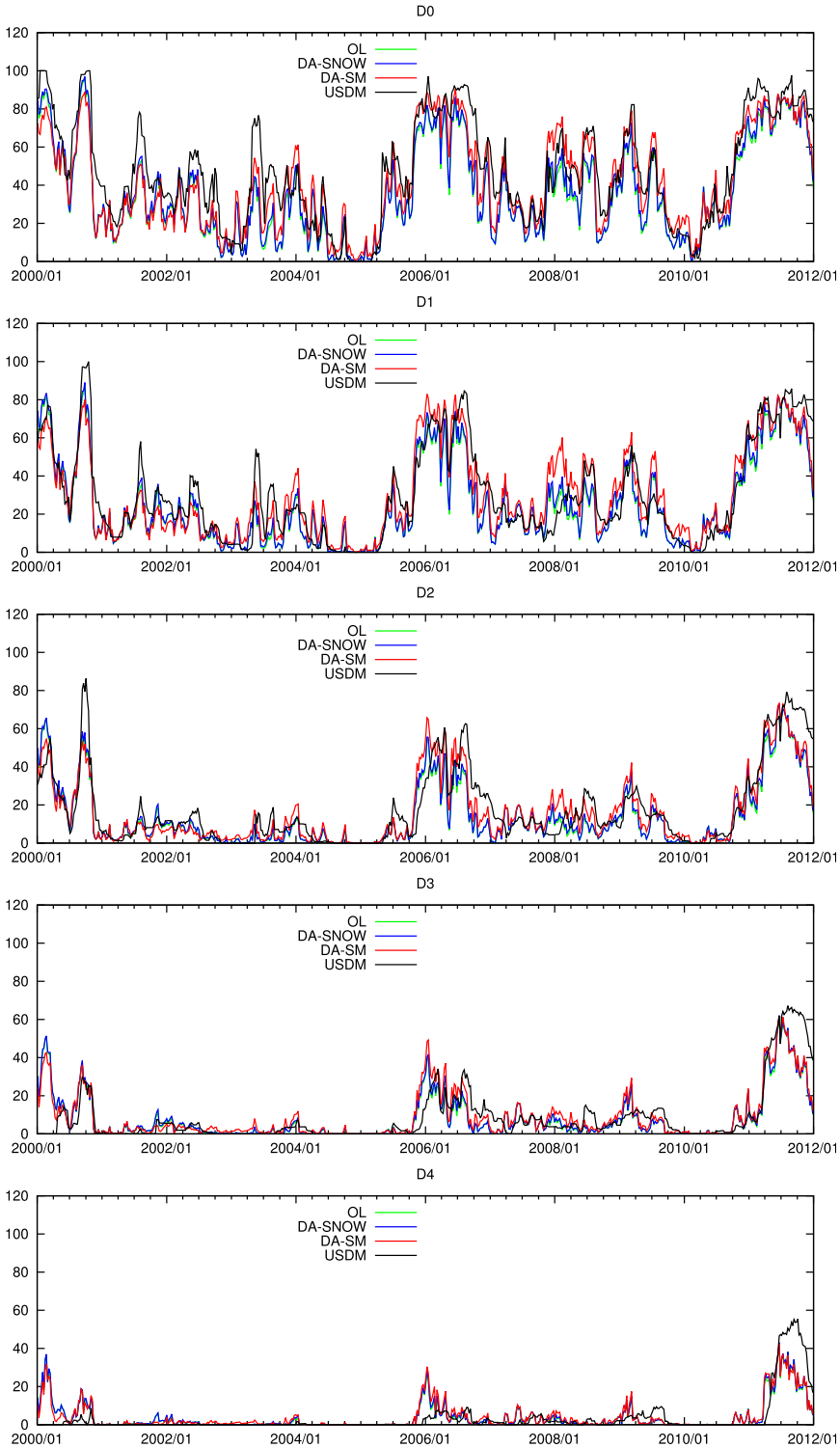

FIG. 9. Time series of the drought area percentage (based on root-zone soil moisture percentiles) from the OL, snow depth (DA-SNOW), and soil moisture (DA-SM) DA integrations for the South region of the United States, and USDM for a time period of 2000–12: (from top to bottom) percentiles D0–D4.

TABLE 5. Comparison of the *R*, RMSE (%), and bias (%) of the drought percentage area (based on root-zone soil moisture percentiles) against the USDM estimates from the OL, soil moisture (DA-SM), and snow depth (DA-SNOW) DA integrations for the six U.S. regions used in the USDM. Statistically significant improvements (degradations) relative to OL at the 5% level are shown in boldface (boldface italic).

	R			RMSE			Bias		
	OL	DA-SM	DA-SNOW	OL	DA-SM	DA-SNOW	OL	DA-SM	DA-SNOW
South									
D0	0.91	0.90	0.91	15.7	**12.8**	15.0	11.2	**5.0**	10.1
D1	0.91	0.89	0.91	11.1	11.1	10.7	4.7	**−0.1**	4.0
D2	0.89	0.89	0.89	9.9	9.2	9.7	3.8	**1.2**	3.3
D3	0.78	0.80	0.78	9.0	8.5	9.0	0.5	−0.7	0.3
D4	0.73	0.73	0.73	6.7	6.7	6.7	−0.4	−0.8	−0.5
Southeast									
D0	0.83	0.85	0.83	22.6	**20.9**	22.3	12.9	**11.2**	12.7
D1	0.79	0.81	0.79	18.0	**16.9**	18.0	6.0	**4.7**	5.9
D2	0.74	0.76	0.75	14.2	13.6	14.1	4.8	3.9	4.8
D3	0.71	0.72	0.71	8.8	8.6	8.8	1.4	0.9	1.3
D4	0.70	0.72	0.70	4.4	4.4	4.4	−0.4	−0.6	−0.4
Northeast									
D0	0.77	0.77	0.77	17.0	17.0	17.5	−6.4	−6.5	−7.5
D1	0.72	0.72	0.72	16.5	16.6	***17.6***	−9.6	−9.7	***−10.6***
D2	0.62	0.63	0.65	12.0	12.0	12.6	−5.7	−5.8	−6.3
D3	0.46	0.46	0.50	9.4	9.4	9.9	−3.8	−3.8	−4.1
D4	0.06	0.06	0.07	5.7	5.8	6.0	−1.8	−1.8	−2.0
Midwest									
D0	0.84	0.82	0.83	10.6	***11.5***	***11.3***	0.2	***−2.7***	***−2.0***
D1	0.81	0.79	0.79	10.2	***12.2***	***11.8***	−5.9	***−8.1***	***−7.5***
D2	0.74	0.71	0.72	7.6	***9.1***	***8.8***	−4.7	***−5.9***	***−5.5***
D3	0.31	0.27	0.30	6.3	***7.3***	***7.1***	−3.5	***−4.2***	***−4.0***
D4	0.16	0.14	0.16	3.3	3.7	3.6	−1.8	−2.0	−2.0
High Plains									
D0	0.66	0.66	0.64	32.1	**27.6**	32.3	25.3	**19.3**	24.9
D1	0.62	0.62	0.55	24.6	**22.3**	25.7	14.3	**10.1**	14.4
D2	0.61	0.57	0.52	19.8	18.9	20.7	11.0	**8.8**	11.2
D3	0.52	0.43	0.46	11.6	11.9	12.1	4.1	3.0	4.3
D4	0.55	0.40	0.54	2.7	3.2	2.6	−0.5	−0.9	−0.4
West									
D0	0.57	0.61	0.51	30.3	**25.9**	***32.2***	24.1	**19.7**	***25.6***
D1	0.54	0.57	0.49	25.3	**23.1**	***26.7***	15.7	**12.4**	16.7
D2	0.53	0.54	0.51	21.9	21.3	22.5	12.6	11.1	13.1
D3	0.51	0.47	0.51	11.9	12.1	12.0	4.0	3.4	4.3
D4	0.43	0.41	0.44	3.9	3.2	3.6	−1.5	−1.6	−1.3

severe drought over Mexico for these three cases). The precipitation data over Mexico in NLDAS-2 is likely to be of lower quality (compared to that over the CONUS) because of the reduced gauge coverage and the lack of the spatial adjustment using PRISM climatology (Xia et al. 2012a). It can be surmised that the corresponding lower quality in the drought estimates is improved by soil moisture DA, though a quantitative evaluation over Mexico is not presented here.

5. Summary

This article examines the impact of incorporating remotely sensed soil moisture and snow depth retrievals for improving land surface model estimates and their subsequent contribution toward improved estimation of agricultural and hydrological droughts. The study is conducted over the CONUS using the NLDAS-2 domain configuration and datasets, with the Noah land surface model. Over a time period from 1979 to 2011, a number of passive microwave–based soil moisture and snow depth datasets is assimilated into the model, using a 1D ensemble Kalman filter algorithm.

The model simulations and the added impact of data assimilation on the land surface model estimates are evaluated using a wide range of independent datasets. Soil moisture estimates from the model integration without data assimilation were found to have high skills

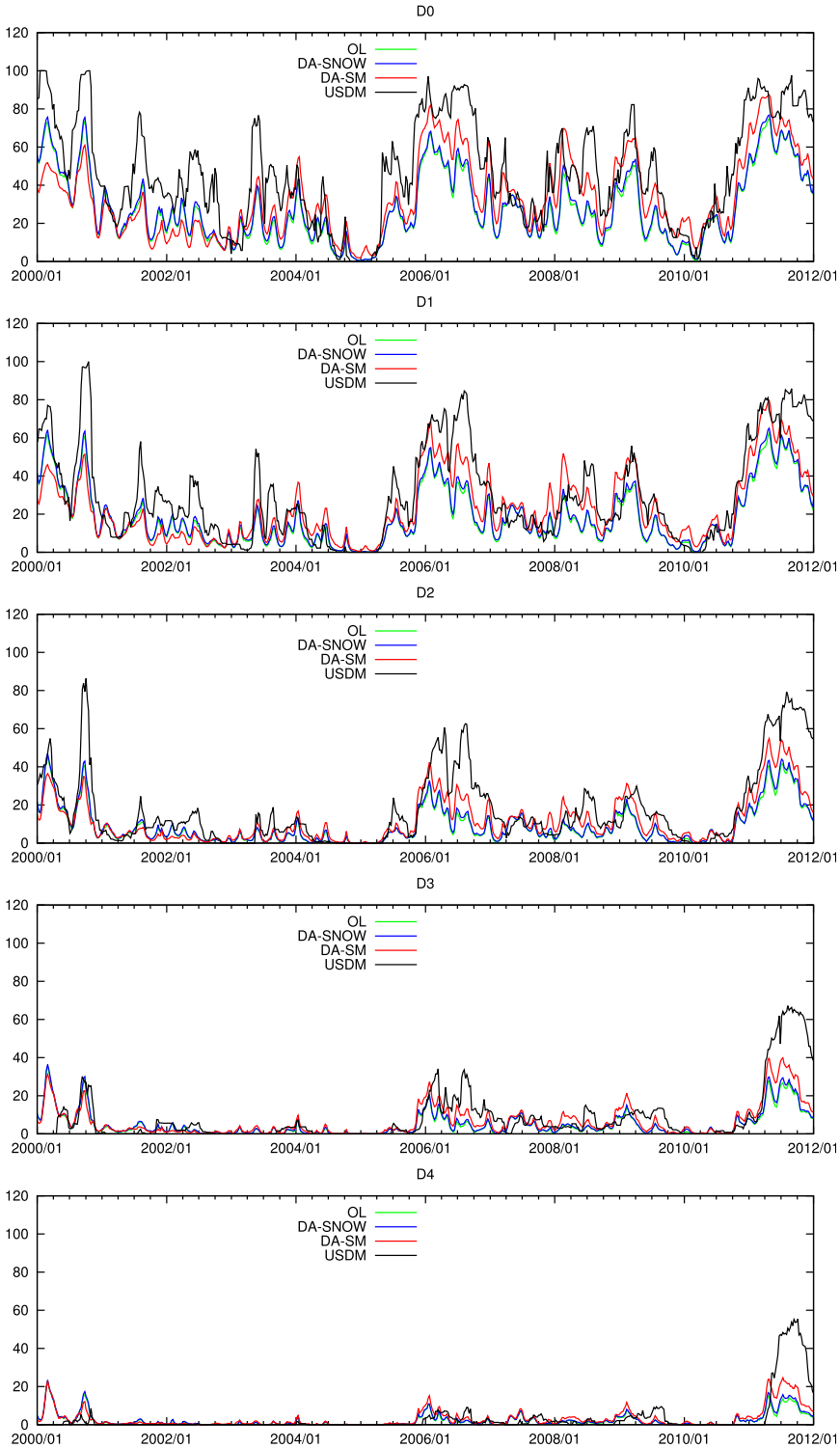

FIG. 10. As in Fig. 9, but for streamflow percentiles.

when compared to the USDA ARS and SCAN in situ soil moisture measurements. Data assimilation provides marginal improvements to these already highly skilled estimates of soil moisture. Snow depth DA integrations were conducted by first augmenting the passive microwave retrievals with available in situ measurements of snow depth from GHCN data. This approach is consistent with earlier studies and the strategy used in several

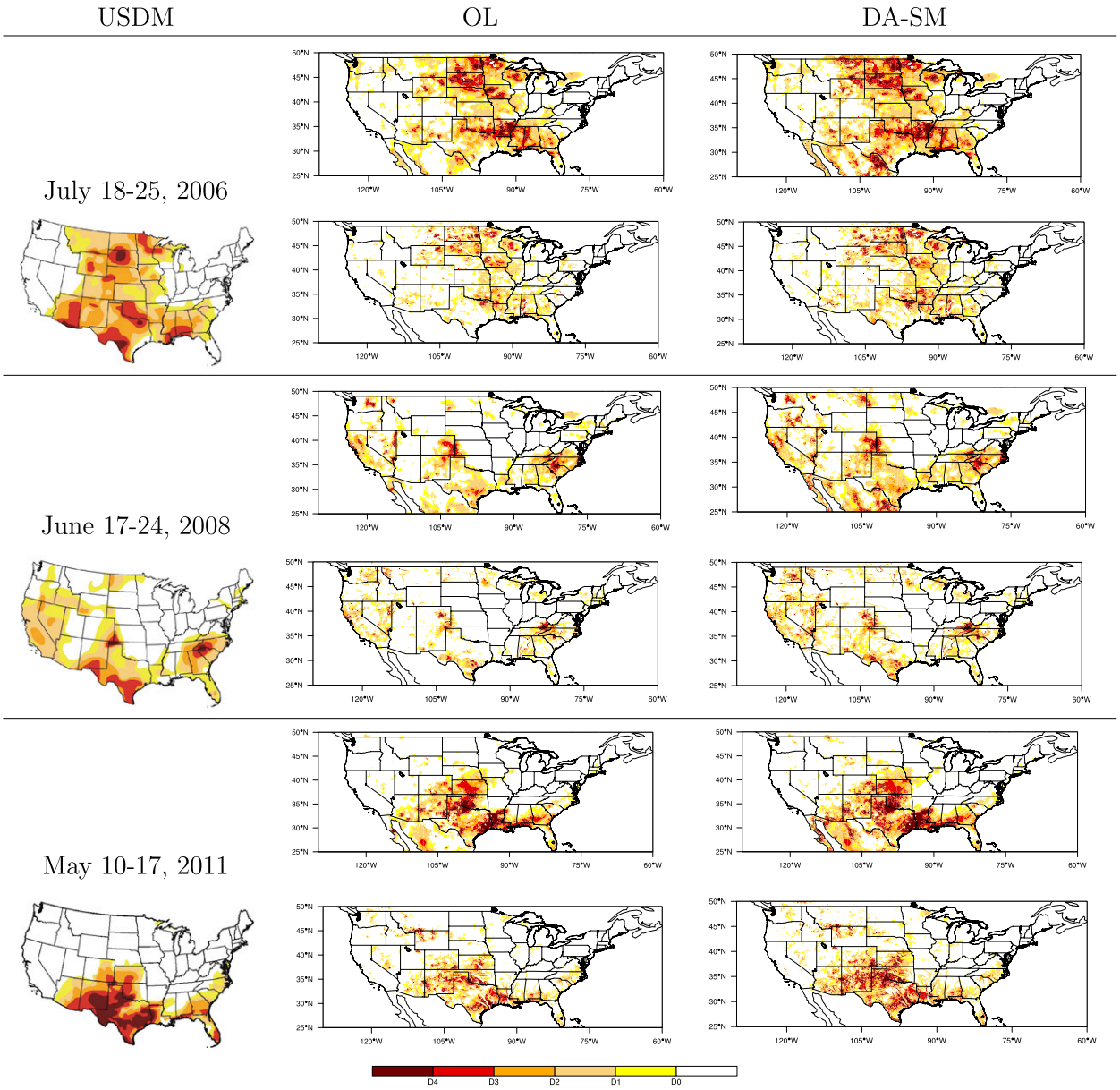

FIG. 11. Comparison of the drought percentile maps from OL and soil moisture DA integrations against the corresponding USDM estimate for (from top to bottom) three representative cases. For each case, the top row represents the root-zone soil moisture–based percentiles and the bottom row represents the streamflow-based percentiles. The colors used to represent the D0–D4 percentiles run from white to brown.

operational agencies to improve the known poor skill of the passive microwave snow depth estimates. To provide an independent assessment of the snow depth fields, analysis products from CMC and SNODAS were used. These comparisons indicate that improvements in snow depth estimates, consistent with CMC and SNODAS products, were obtained from assimilation.

To provide an independent measure of the improvements from data assimilation, we examined the impacts on the routed streamflow estimates by comparing them to the streamflow measurements from available unregulated USGS stations. The improvements from both sets of assimilation were minor across most basins, with soil moisture DA providing more consistent improvements by improving R, RMSE, and NSE metrics over the open loop. The downstream impacts in streamflow due to snow depth DA were mixed, with an overall degradation in the RMSE and NSE skill metrics. Some of the significant

degradation in streamflow due to snow depth DA was observed over the western United States, indicating that additional enhancements (either gauge or ancillary data based) to the snow depth retrievals and/or bias correction methodologies may be required in those regions.

The influence of data assimilation on improving drought estimates was examined using the root-zone soil moisture– and streamflow-based percentiles. As the time period of data (1979–2011) can be considered rather short for the computation of percentiles, we employ a 5-day moving window approach to increase the sampling density in these calculations. A quantitative evaluation of the percentage area in drought for five drought severity categories was examined by comparing the model-based estimates against corresponding USDM archived data. Over areas with warm climate and seasons (such as the South region of the USDM), root-zone soil moisture–based percentiles sufficiently capture the spatial distribution and intensities of drought, as evidenced from the high skills of the OL integration. Soil moisture DA provided added improvements to the percent area estimates with smaller enhancements for more severe drought categories. Improvements in the representation of spatial patterns of drought were also obtained from soil moisture DA. The impact of snow depth DA, however, was small and in many instances was found to cause degradations in the estimates of drought area percentages.

In the drought evaluations, we directly compare the root-zone soil moisture–based and streamflow-percentile-based drought area to the USDM data. As the operational USDM data are generated using a blend of different indicators and subjective analysis, we do not expect our single-variable-based drought estimates to match the USDM perfectly. The results in Fig. 9, however, support our basic methodology that soil moisture percentiles are a primary indicator of drought in warm seasons and climates. In other regions, a blend of different indices may be more appropriate if direct comparisons to the USDM are employed, as done in more recent studies, such as Xia et al. (2014).

Our results also indicate that the improvements in drought estimation from soil moisture DA were largely at short time scales. This was expected as the strategy of scaling observations for a priori bias correction prevents changes in the model climatology and assimilation impacts at long time scales. Development and application of DA techniques that include notions for handling biases during data assimilation may be required if data assimilation is employed for generating trends at longer time scales.

The data assimilation experiments presented in this article employed separate instances for soil moisture and snow depth DA, which are helpful for isolating the impact of each assimilation scenario in different seasons and geographic regions. The present study is therefore an important step toward the development of a system that is capable of simultaneously assimilating both types of data, which is left for future work.

Acknowledgments. Funding for this work was provided by the NASA Science Mission Directorate's Earth Science Division through the National Climate Assessment (NCA) project. Computing was supported by the resources at the NASA Center for Climate Simulation. The NLDAS-2 forcing data used in this effort were acquired as part of the activities of NASA's Science Mission Directorate and are archived and distributed by the Goddard Earth Sciences (GES) Data and Information Services Center (DISC). Part of the funding for this effort was provided by NOAA's Climate Program Office MAPP program. Rolf Reichle was supported by the NASA program on the Science of *Terra* and *Aqua*. We are grateful to Dr. Gabrielle De Lannoy for the assistance with the reprocessed and quality-controlled SCAN soil moisture dataset and to Drs. Dorothy Hall and James Foster for their help with the development of snow depth retrieval products.

REFERENCES

Andreadis, K., and D. Lettenmaier, 2006: Assimilating remotely sensed snow observations into a macroscale hydrology model. *Adv. Water Resour.,* **29,** 872–886, doi:10.1016/j.advwatres.2005.08.004.

Arsenault, K., P. Houser, G. De Lannoy, and P. Dirmeyer, 2013: Impacts of snow cover fraction data assimilation on modeled energy and moisture budgets. *J. Geophys. Res. Atmos.,* **118,** 7489–7504, doi:10.1002/jgrd.50542.

Bales, R., N. Molotch, T. Painter, M. Dettinger, R. Rice, and J. Dozier, 2006: Mountain hydrology of the western United States. *Water Resour. Res.,* **42,** W08432, doi:10.1029/2005WR004387.

Barlage, M., and Coauthors, 2010: Noah land surface model modifications to improve snowpack prediction in the Colorado Rocky Mountains. *J. Geophys. Res.,* **115,** D22101, doi:10.1029/2009JD013470.

Barnett, T., J. Adam, and D. Lettenmaier, 2005: Potential impacts of a warming climate on water availability in snow-dominated regions. *Nature,* **428,** 303–309, doi:10.1038/nature04141.

Barrett, A., 2003: National Operational Hydrologic Remote Sensing Snow Data Assimilation System (SNODAS) products at NSIDC. Special Rep. 11, NSIDC, Boulder, CO, 19 pp. [Available online at https://nsidc.org/pubs/documents/special/nsidc_special_report_11.pdf.]

Berg, A., and K. Mulroy, 2006: Streamflow predictability in the Saskatchewan/Nelson River basin given macroscale estimates of initial soil moisture. *Hydrol. Sci.,* **51,** 642–654, doi:10.1623/hysj.51.4.642.

Bissolli, P., and U. Maier, 2009: SnowClim: Snow climate monitoring for Europe. *Abstracts, Ninth EMS Annual Meeting/Ninth*

European Conf. on Applications of Meteorology, Toulouse, France, EMS, EMS2009-530. [Available online at http://meetingorganizer.copernicus.org/EMS2009/EMS2009-530.pdf.]

Bolten, J., and W. Crow, 2012: Improved prediction of quasi-global vegetation conditions using remotely-sensed surface soil moisture. *Geophys. Res. Lett.,* **39,** L19406, doi:10.1029/2012GL053470.

Boone, A., and Coauthors, 2004: The Rhône-Aggregation land surface scheme intercomparison project: An overview. *J. Climate,* **17,** 187–208, doi:10.1175/1520-0442(2004)017<0187:TRLSSI>2.0.CO;2.

Brasnett, B., 1999: A global analysis of snow depth for numerical weather prediction. *J. Appl. Meteor.,* **38,** 726–740, doi:10.1175/1520-0450(1999)038<0726:AGAOSD>2.0.CO;2.

Brown, R., and R. Braaten, 1998: Spatial and temporal variability of Canadian monthly snow depths. *Atmos.–Ocean,* **36,** 37–45, doi:10.1080/07055900.1998.9649605.

——, and B. Brasnett, 2010: Canadian Meteorological Centre (CMC) daily snow depth analysis data. National Snow and Ice Data Center, Boulder, CO, digital media. [Available online at http://nsidc.org/data/nsidc-0447.]

Carroll, T., D. Cline, G. Fall, A. Nilsson, L. Li, and A. Rost, 2001: NOHRSC operations and the simulation of snow cover properties for the conterminous U.S. *Proc. 69th Annual Meeting of the Western Snow Conf.,* Sun Valley, ID, Western Snow Conference, 14 pp.

Chang, A., J. Foster, and D. Hall, 1987: *Nimbus-7* SMMR derived global snow cover parameters. *Ann. Glaciol.,* **9,** 39–44.

Cordisco, A., C. Prigent, and F. Aires, 2006: Snow characterization at a global scale with passive microwave satellite observations. *J. Geophys. Res.,* **111,** D19102, doi:10.1029/2005JD006773.

Cressman, G., 1959: An operational objective analysis system. *Mon. Wea. Rev.,* **87,** 367–374, doi:10.1175/1520-0493(1959)087<0367:AOOAS>2.0.CO;2.

Crow, W., and E. Wood, 2003: The assimilation of remotely sensed soil brightness temperature imagery into a land surface model using ensemble Kalman filtering: A case study based on ESTAR measurements during SGP97. *Adv. Water Resour.,* **26,** 137–149, doi:10.1016/S0309-1708(02)00088-X.

——, R. Bindlish, and T. Jackson, 2005: The added value of spaceborne passive microwave soil moisture retrievals for forecasting rainfall–runoff ratio partitioning. *Geophys. Res. Lett.,* **32,** L18401, doi:10.1029/2005GL023543.

Dechant, C., and H. Moradkhani, 2011: Radiance data assimilation for operational snow and streamflow forecasting. *Adv. Water Resour.,* **34,** 351–364, doi:10.1016/j.advwatres.2010.12.009.

De Lannoy, G., R. Reichle, K. Arsenault, P. Houser, S. Kumar, N. Verhoest, and V. Pauwels, 2012: Multiscale assimilation of Advanced Microwave Scanning Radiometer–EOS snow water equivalent and Moderate Resolution Imaging Spectroradiometer snow cover fraction observations in northern Colorado. *Water Resour. Res.,* **48,** W01522, doi:10.1029/2011WR010588.

de Rosnay, P., G. Balsamo, A. Albergel, J. Munoz-Sabater, and L. Isaksen, 2013: Initialisation of land surface variables for Numerical Weather Prediction. *Surv. Geophys.,* **35,** 607–621, doi:10.1007/s10712-012-9207-x.

Dong, J., J. Walker, and P. Houser, 2005: Factors affecting remotely sensed snow water equivalent uncertainty. *Remote Sens. Environ.,* **97,** 68–82, doi:10.1016/j.rse.2005.04.010.

——, ——, ——, and C. Sun, 2007: Scanning multichannel microwave radiometer snow water equivalent assimilation. *J. Geophys. Res.,* **112,** D07108, doi:10.1029/2006JD007209.

Draper, C., J. Mahfouf, and J. Walker, 2011: Root zone soil moisture from the assimilation of screen-level variables and remotely sensed soil moisture. *J. Geophys. Res.,* **116,** D02127, doi:10.1029/2010JD013829.

——, R. Reichle, G. De Lannoy, and Q. Liu, 2012: Assimilation of passive and active microwave soil moisture retrievals. *Geophys. Res. Lett.,* **39,** L04401, doi:10.1029/2011GL050655.

Dressier, K., G. Leavesley, R. Bales, and S. Fassnacht, 2004: Streamflow estimation from hydrologic model assimilation of remotely sensed snow information in snowmelt dominated basins. *Eos, Trans. Amer. Geophys. Union,* **85** (Fall Meeting Suppl.), Abstract C31A-0288.

Drusch, M., D. Vasiljevic, and P. Viterbo, 2004: ECMWF's global snow analysis: Assessment and revision based on satellite observations. *J. Appl. Meteor.,* **43,** 1282–1294, doi:10.1175/1520-0450(2004)043<1282:EGSAAA>2.0.CO;2.

——, E. Wood, and H. Gao, 2005: Observation operators for the direct assimilation of TRMM microwave imager retrieved soil moisture. *Geophys. Res. Lett.,* **32,** L15403, doi:10.1029/2005GL023623.

Ek, M., K. Mitchell, L. Yin, P. Rogers, P. Grunmann, V. Koren, G. Gayno, and J. Tarpley, 2003: Implementation of Noah land-surface model advances in the NCEP operational mesoscale Eta model. *J. Geophys. Res.,* **108,** 8851, doi:10.1029/2002JD003296.

——, and Coauthors, 2011: North American Land Data Assimilation System Phase 2 (NLDAS-2): Development and applications. *GEWEX News,* Vol. 21, No. 2, International GEWEX Project Office, Silver Spring, MD, 6–7. [Available online at www.gewex.org/gewexnews/May2011.pdf.]

Entekhabi, D., R. Reichle, R. Koster, and W. Crow, 2010a: Performance metrics for soil moisture retrievals and application requirements. *J. Hydrometeor.,* **11,** 832–840, doi:10.1175/2010JHM1223.1.

——, and Coauthors, 2010b: The Soil Moisture Active Passive (SMAP) Mission. *Proc. IEEE,* **98,** 704–716, doi:10.1109/JPROC.2010.2043918.

Ferguson, R., 1985: Runoff from glacierized mountains: A model for annual variation and its forecasting. *Water Resour. Res.,* **21,** 702–708, doi:10.1029/WR021i005p00702.

Ffolliott, P., G. Gottfried, and M. Baker, 1989: Water yield from forest snowpack management: Research findings in Arizona and New Mexico. *Water Resour. Res.,* **25,** 1999–2007, doi:10.1029/WR025i009p01999.

Foster, J., A. Chang, and D. Hall, 1997: Comparison of snow mass estimates from a prototype passive microwave snow algorithm, a revised algorithm and a snow depth climatology. *Remote Sens. Environ.,* **62,** 132–142, doi:10.1016/S0034-4257(97)00085-0.

——, C. Sun, J. Walker, R. Kelly, A. Chang, J. Dong, and H. Powell, 2005: Quantifying the uncertainty in passive microwave snow water equivalent observations. *Remote Sens. Environ.,* **94,** 187–203, doi:10.1016/j.rse.2004.09.012.

Franz, K., and S. Sorooshian, 2008: Operational snow modeling: Addressing the challenges of an energy balance model for National Weather Service forecasts. *J. Hydrol.,* **360,** 48–66, doi:10.1016/j.jhydrol.2008.07.013.

Hain, C., W. Crow, M. Anderson, and J. Mecikalski, 2012: An ensemble Kalman filter dual assimilation of thermal infrared and microwave satellite observations of soil moisture into the

Noah land surface model. *Water Resour. Res.,* **48,** W11517, doi:10.1029/2011WR011268.

He, M., T. Hogue, S. Margulis, and K. Franz, 2011: An integrated uncertainty and ensemble-based data assimilation approach for improved operational streamflow predictions. *Hydrol. Earth Syst. Sci. Discuss.,* **8,** 7709–7755, doi:10.5194/hessd-8-7709-2011.

Heim, R., 2002: A review of twentieth-century drought indices used in the United States. *Bull. Amer. Meteor. Soc.,* **83,** 1149–1165.

Jackson, T. J., 1993: Measuring surface soil moisture using passive microwave remote sensing. *Hydrol. Processes,* **7,** 139–152, doi:10.1002/hyp.3360070205.

——, and Coauthors, 2010: Validation of Advanced Microwave Scanning Radiometer soil moisture products. *IEEE Trans. Geosci. Remote Sens.,* **48,** 4256–4272, doi:10.1109/TGRS.2010.2051035.

Kelly, R., 2009: The AMSR-E snow depth algorithm: Description and initial results. *J. Remote Sens. Soc. Japan,* **29,** 307–317, doi:10.11440/rssj.29.307.

——, A. Chang, L. Tsang, and J. Foster, 2003: A prototype AMSR-E global snow area and snow depth algorithm. *IEEE Trans. Geosci. Remote Sens.,* **41,** 230–242, doi:10.1109/TGRS.2003.809118.

Keyantash, J., and J. Dracup, 2002: The quantification of drought: An evaluation of drought indices. *Bull. Amer. Meteor. Soc.,* **83,** 1167–1180.

Koster, R., S. Mahanama, B. Livneh, D. Lettenmaier, and R. Reichle, 2010: Skill in streamflow forecasts derived from large-scale estimates of soil moisture and snow. *Nat. Geosci.,* **3,** 613–616, doi:10.1038/ngeo944.

——, G. Walker, S. Mahanama, and R. Reichle, 2014: Soil moisture initialization error and subgrid variability of precipitation in seasonal streamflow forecasting. *J. Hydrometeor.,* **15,** 69–88, doi:10.1175/JHM-D-13-050.1.

Krenke, A., 2004: Former Soviet Union hydrological snow surveys, 1966–1996. National Snow and Ice Data Center, Boulder, CO, digital media. [Available online at http://nsidc.org/data/g01170.]

Kumar, S., and Coauthors, 2006: Land Information System: An interoperable framework for high resolution land surface modeling. *Environ. Modell. Software,* **21,** 1402–1415, doi:10.1016/j.envsoft.2005.07.004.

——, R. Reichle, C. Peters-Lidard, R. Koster, X. Zhan, W. Crow, J. Eylander, and P. Houser, 2008: A land surface data assimilation framework using the Land Information System: Description and applications. *Adv. Water Resour.,* **31,** 1419–1432, doi:10.1016/j.advwatres.2008.01.013.

——, ——, R. Koster, W. Crow, and C. Peters-Lidard, 2009: Role of subsurface physics in the assimilation of surface soil moisture observations. *J. Hydrometeor.,* **10,** 1534–1547, doi:10.1175/2009JHM1134.1.

——, C. Peters-Lidard, J. Santanello, K. Harrison, Y. Liu, and M. Shaw, 2012a: Land surface Verification Toolkit (LVT)—A generalized framework for land surface model evaluation. *Geosci. Model Dev.,* **5,** 869–886, doi:10.5194/gmd-5-869-2012.

——, R. Reichle, K. Harrison, C. Peters-Lidard, S. Yatheendradas, and J. Santanello, 2012b: A comparison of methods for a priori bias correction in soil moisture data assimilation. *Water Resour. Res.,* **48,** W03515, doi:10.1029/2010WR010261.

Liu, Q., and Coauthors, 2011: The contributions of precipitation and soil moisture observations to the skill of soil moisture estimates in a land data assimilation system. *J. Hydrometeor.,* **12,** 750–765, doi:10.1175/JHM-D-10-05000.1.

Liu, Y., R. Parinussa, W. Dorigo, R. De Jeu, W. Wagner, A. Van Dijk, M. McCabe, and J. Evans, 2011: Developing an improved soil moisture dataset by blending passive and active microwave satellite-based retrievals. *Hydrol. Earth Syst. Sci.,* **15,** 425–436, doi:10.5194/hess-15-425-2011.

——, C. Peters-Lidard, S. Kumar, J. Foster, M. Shaw, Y. Tian, and G. Fall, 2013: Assimilating satellite-based snow depth and snow cover products for improving snow predictions in Alaska. *Adv. Water Resour.,* **54,** 208–227, doi:10.1016/j.advwatres.2013.02.005.

Livneh, B., Y. Xia, K. Mitchell, M. Ek, and D. Lettenmaier, 2010: Noah LSM snow model diagnostics and enhancements. *J. Hydrometeor.,* **11,** 721–738, doi:10.1175/2009JHM1174.1.

Lohmann, D., R. Nolte-Holube, and E. Raschke, 1996: A large-scale horizontal routing model to be coupled to land surface parameterization schemes. *Tellus,* **48A,** 708–721, doi:10.1034/j.1600-0870.1996.t01-3-00009.x.

——, and Coauthors, 1998: The project for intercomparison of land-surface parameterization schemes (PILPS) phase 2(c) Red–Arkansas River basin experiment: 3. Spatial and temporal analysis of water fluxes. *Global Planet. Change,* **19,** 161–179, doi:10.1016/S0921-8181(98)00046-0.

——, and Coauthors, 2004: Streamflow and water balance intercomparisons of four land surface models in the North American Land Data Assimilation System project. *J. Geophys. Res.,* **109,** D07S91, doi:10.1029/2003JD003517.

Mahanama, S., R. Koster, R. Reichle, and L. Zubair, 2008: The role of soil moisture initialization in subseasonal and seasonal streamflow prediction—A case study in Sri Lanka. *Adv. Water Resour.,* **31,** 1333–1343, doi:10.1016/j.advwatres.2008.06.004.

——, B. Livneh, R. Koster, D. Lettenmaier, and R. Reichle, 2012: Soil moisture, snow, and seasonal streamflow forecasts in the United States. *J. Hydrometeor.,* **13,** 189–203, doi:10.1175/JHM-D-11-046.1.

Margulis, S., D. McLaughlin, D. Entekhabi, and S. Dunne, 2002: Land data assimilation and estimation of soil moisture using measurements from the Southern Great Plains 1997 Field Experiment. *Water Resour. Res.,* **38,** 1299, doi:10.1029/2001WR001114.

Markus, T., D. Powell, and J. Wang, 2006: Sensitivity of passive microwave snow depth retrievals to weather effects and snow evolution. *IEEE Trans. Geosci. Remote Sens.,* **44,** 68–77, doi:10.1109/TGRS.2005.860208.

Matsui, T., D. Mocko, M.-I. Lee, M. Suarez, and R. Pielke Sr., 2010: Ten-year climatology of summertime diurnal rainfall rate over the conterminous U.S. *Geophys. Res. Lett.,* **37,** L13807, doi:10.1029/2010GL044139.

Maurer, E. P., and D. P. Lettenmaier, 2003: Predictability of seasonal runoff in the Mississippi River basin. *J. Geophys. Res.,* **108,** 8607, doi:10.1029/2002JD002555.

Menne, M. J., I. Durre, R. S. Vose, B. E. Gleason, and T. G. Houston, 2012: An overview of the global historical climatology network-daily database. *J. Atmos. Oceanic Technol.,* **29,** 897–910, doi:10.1175/JTECH-D-11-00103.1.

Mitchell, K. E., and Coauthors, 2004: The multi-institution North American Land Data Assimilation System (NLDAS): Utilization of multiple GCIP products and partners in a continental distributed hydrological modeling system. *J. Geophys. Res.,* **109,** D07S90, doi:10.1029/2003JD003823.

Mo, K., 2008: Model-based drought indices over the United States. *J. Hydrometeor.,* **9,** 1212–1230, doi:10.1175/2008JHM1002.1.

Mote, P., A. Hamlet, M. Clark, and D. Lettenmaier, 2005: Declining mountain snowpack in western North America. *Bull. Amer. Meteor. Soc.,* **86,** 39–49, doi:10.1175/BAMS-86-1-39.

Nagarajan, K., J. Judge, A. Monsivais-Huertero, and W. Graham, 2012: Impact of assimilating passive microwave observations on root-zone soil moisture under dynamic vegetation conditions. *IEEE Trans. Geosci. Remote Sens.,* **50,** 4279–4291, doi:10.1109/TGRS.2012.2191154.

Nijssen, B., D. Lettenmaier, X. Liang, S. Wetzel, and E. Wood, 1997: Streamflow simulation for continental-scale river basins. *Water Resour. Res.,* **33,** 711–724, doi:10.1029/96WR03517.

Njoku, E. G., and D. Entekhabi, 1996: Passive microwave remote sensing of soil moisture. *J. Hydrol.,* **184,** 101–130, doi:10.1016/0022-1694(95)02970-2.

Owe, M., R. de Jeu, and T. Holmes, 2008: Multisensor historical climatology of satellite-derived global land surface moisture. *J. Geophys. Res.,* **113,** F01002, doi:10.1029/2007JF000769.

Parajka, J., V. Naemi, G. Bloschl, W. Wagner, R. Merz, and L. Scipal, 2006: Assimilating scatterometer soil moisture data into conceptual hydrologic models at coarse scales. *Hydrol. Earth Syst. Sci.,* **10,** 353–368, doi:10.5194/hess-10-353-2006.

Pauwels, R., R. Hoeben, N. Verhoest, F. De Troch, and P. Troch, 2002: Improvements of TOPLATS-based discharge predictions through assimilation of ERS-based remotely sensed soil moisture values. *Hydrol. Processes,* **16,** 995–1013, doi:10.1002/hyp.315.

Peters-Lidard, C. D., and Coauthors, 2007: High-performance Earth System modeling with NASA/GSFC's Land Information System. *Innovations Syst. Software Eng.,* **3** (3), 157–165, doi:10.1007/s11334-007-0028-x.

——, S. Kumar, D. Mocko, and Y. Tian, 2011: Estimating evapotranspiration with land data assimilation systems. *Hydrol. Processes,* **25,** 3979–3992, doi:10.1002/hyp.8387.

Pomeroy, J., and D. Gray, 1995: *Snowcover Accumulation, Relocation and Management.* National Hydrology Research Institute, 350 pp.

Pulliainen, J., 2006: Mapping of snow water equivalent and snow depth in boreal and sub-arctic zones by assimilating spaceborne microwave radiometer data and ground-based observations. *Remote Sens. Environ.,* **101,** 257–269, doi:10.1016/j.rse.2006.01.002.

——, and M. Hallikainen, 2001: Retrieval of regional snow water equivalent from spaceborne passive microwave observations. *Remote Sens. Environ.,* **75,** 76–85, doi:10.1016/S0034-4257(00)00157-7.

Rango, A., V. Salomonson, and J. Foster, 1977: Seasonal streamflow estimation in the Himalayan region employing meteorological satellite snow cover observations. *Water Resour. Res.,* **13,** 109–112, doi:10.1029/WR013i001p00109.

Reichle, R., 2008: Data assimilation methods in the Earth sciences. *Adv. Water Resour.,* **31,** 1411–1418, doi:10.1016/j.advwatres.2008.01.001.

——, and R. Koster, 2004: Bias reduction in short records of satellite soil moisture. *Geophys. Res. Lett.,* **31,** L19501, doi:10.1029/2004GL020938.

——, and ——, 2005: Global assimilation of satellite surface soil moisture retrievals into the NASA Catchment land surface model. *Geophys. Res. Lett.,* **32,** L02404, doi:10.1029/2004GL021700.

——, D. McLaughlin, and D. Entekhabi, 2002a: Hydrologic data assimilation with the ensemble Kalman filter. *Mon. Wea. Rev.,* **130,** 103–114, doi:10.1175/1520-0493(2002)130<0103:HDAWTE>2.0.CO;2.

——, J. Walker, R. Koster, and P. Houser, 2002b: Extended vs. ensemble Kalman filtering. *J. Hydrometeor.,* **3,** 728–740, doi:10.1175/1525-7541(2002)003<0728:EVEKFF>2.0.CO;2.

——, R. Koster, P. Liu, S. P. P. Mahanama, E. G. Njoku, and M. Owe, 2007: Comparison and assimilation of global soil moisture retrievals from the Advanced Microwave Scanning Radiometer for the Earth Observing System (AMSR-E) and the Scanning Multichannel Microwave Radiometer (SMMR). *J. Geophys. Res.,* **112,** D09108, doi:10.1029/2006JD008033.

——, S. Kumar, S. Mahanama, R. Koster, and Q. Liu, 2010: Assimilation of satellite-derived skin temperature observations into land surface models. *J. Hydrometeor.,* **11,** 1103–1122, doi:10.1175/2010JHM1262.1.

Rodell, M., and P. Houser, 2004: Updating a land surface model with MODIS-derived snow cover. *J. Hydrometeor.,* **5,** 1064–1075, doi:10.1175/JHM-395.1.

——, and Coauthors, 2004: The Global Land Data Assimilation System. *Bull. Amer. Meteor. Soc.,* **85,** 381–394, doi:10.1175/BAMS-85-3-381.

Ross, B., and B. Brasnett, 2010: Canadian Meteorological Centre (CMC) daily snow depth analysis data. National Snow and Ice Data Center, Boulder, CO, digital media. [Available online at http://nsidc.org/data/nsidc-0447.]

Roy, A., A. Royer, and R. Turcotte, 2010: Improvement of springtime streamflow simulations in a boreal environment by incorporating snow covered area derived from remote sensing data. *J. Hydrol.,* **390,** 35–44, doi:10.1016/j.jhydrol.2010.06.027.

Schaefer, G., M. Cosh, and T. Jackson, 2007: The USDA natural resources conservation service soil climate analysis network (SCAN). *J. Atmos. Oceanic Technol.,* **24,** 2073–2077, doi:10.1175/2007JTECHA930.1.

Schlosser, C., A. Robock, K. Vinnikov, N. Speranskaya, and Y. Xue, 1997: 18-year land surface hydrology model simulations for a midlatitude grassland catchment in Valdai, Russia. *Mon. Wea. Rev.,* **125,** 3279–3296, doi:10.1175/1520-0493(1997)125<3279:YLSHMS>2.0.CO;2.

Sheffield, J., Y. Xia, L. Luo, E. Wood, M. Ek, and K. Mitchell, 2012: North American Land Data Assimilation System (NLDAS): A framework for merging model and satellite data for improved drought monitoring. *Remote Sensing of Drought: Innovative Monitoring Approaches,* B. Wardlow, M. Anderson, and J. Verdin, Eds., Taylor and Francis, 227–260.

Shukla, S., and A. Wood, 2008: Use of a standardized runoff index for characterizing hydrologic drought. *Geophys. Res. Lett.,* **35,** L02405, doi:10.1029/2007GL032487.

Slater, A., and M. Clark, 2006: Snow data assimilation via an ensemble Kalman filter. *J. Hydrometeor.,* **7,** 478–493, doi:10.1175/JHM505.1.

Svoboda, M., and Coauthors, 2002: The Drought Monitor. *Bull. Amer. Meteor. Soc.,* **83,** 1181–1190.

Tedesco, M., and P. Narvekar, 2010: Assessment of the NASA AMSRE-E SWE product. *IEEE J. Sel. Top. Appl. Earth Obs. Remote Sens.,* **3,** 141–159, doi:10.1109/JSTARS.2010.2040462.

——, R. Reichle, A. Low, T. Markus, and J. Foster, 2010: Dynamic approaches for snow depth retrieval from spaceborne microwave brightness temperature. *IEEE Trans. Geosci. Remote Sens.,* **48,** 1955–1967, doi:10.1109/TGRS.2009.2036910.

Thirel, G., P. Salamon, P. Burek, and M. Kalas, 2011: Assimilation of MODIS snow cover area data in a distributed hydrological model. *Hydrol. Earth Syst. Sci. Discuss.,* **8,** 1329–1364, doi:10.5194/hessd-8-1329-2011.

Wang, Z., X. Zeng, and M. Decker, 2010: Improving snow processes in the Noah land surface model. *J. Geophys. Res.,* **115,** D20108, doi:10.1029/2009JD013761.

Wood, A. W., A. Kumar, and D. P. Lettenmaier, 2005: A retrospective assessment of National Centers for Environmental Prediction climate model–based ensemble hydrologic forecasting in the western United States. *J. Geophys. Res.,* **110,** D04105, doi:10.1029/2004JD004508.

Xia, Y., M. Ek, H. Wei, and J. Meng, 2012a: Comparative analysis of relationships between NLDAS-2 forcings and model outputs. *Hydrol. Processes,* **26,** 467–474, doi:10.1002/hyp.8240.

——, and Coauthors, 2012b: Continental-scale water and energy flux analysis and validation for the North American Land Data Assimilation System project phase 2 (NLDAS-2): 1. Intercomparison and application of model products. *J. Geophys. Res.,* **117,** D03109, doi:10.1029/2011JD016048.

——, and Coauthors, 2012c: Continental-scale water and energy flux analysis and validation for North American Land Data Assimilation System project phase 2 (NLDAS-2): 2. Validation of model-simulated streamflow. *J. Geophys. Res.,* **117,** D03110, doi:10.1029/2011JD016051.

——, M. Ek, C. Peters-Lidard, D. Mocko, M. Svoboda, J. Sheffield, and E. Wood, 2014: Application of USDM statistics in NLDAS-2: Optimal blended NLDAS drought index over the continental United States. *J. Geophys. Res. Atmos.,* **119,** 2947–2965, doi:10.1002/2013JD020994.

Yang, D., Y. Zhao, R. Armstrong, D. Robinson, and M.-J. Brodzik, 2007: Streamflow response to seasonal snow cover mass changes over large Siberian watersheds. *J. Geophys. Res.,* **112,** F02S22, doi:10.1029/2006JF000518.

Yatheendradas, Y., and Coauthors, 2012: Distributed assimilation of satellite-based snow extent for improving simulated streamflow in mountainous, dense forests: An example over the DMIP2 western basins. *Water Resour. Res.,* **48,** W09557, doi:10.1029/2011WR011347.

Zaitchik, B., and M. Rodell, 2009: Forward-looking assimilation of MODIS-derived snow covered area into a land surface model. *J. Hydrometeor.,* **10,** 130–148, doi:10.1175/2008JHM1042.1.

——, ——, and F. Olivera, 2010: Evaluation of the Global Land Data Assimilation System using global river discharge data and a source-to-sink routing scheme. *Water Resour. Res.,* **46,** W06507, doi:10.1029/2009WR007811.